MASSACHUSETTS INSTITUTE OF TECHNOLOGY

HYDRODYNAMICS LABORATORY

DEPARTMENT OF CIVIL AND SANITARY ENGINEERING

TECHNICAL REPORT No. 8

MEASUREMENTS OF FLUID FRICTION WITH STEADY AND UNSTEADY MOTION

BY

JAMES W. DAILY AND KENNETH C. DEEMER

JULY 1952

PREPARED UNDER

CONTRACT N5ORI - 07826

NR-062 - 047

OFFICE OF NAVAL RESEARCH

U. S. DEPARTMENT OF THE NAVY

WASHINGTON, D. C.

HYDRODYNAMICS LABORATORY
Department of Civil and Sanitary Engineering
Massachusetts Institute of Technology

MEASUREMENTS OF FLUID FRICTION WITH STEADY AND UNSTEADY MOTION

by

James W. Daily and Kenneth C. Deemer

July 1952

Prepared under
Contract N5ori-07826, NR-062-047
Office of Naval Research
U. S. Department of the Navy
Washington, D. C.

ACKNOWLEDGMENT

The investigation described in this report is being conducted under the sponsorship of the Office of Naval Research under Contract No. N5ori-07826, NR-062-047 with M.I.T. The initial phase of this study was covered in a previous report: "The Unsteady Flow Water Tunnel at the Massachusetts Institute of Technology."

Dr. Arthur T. Ippen, Professor of Hydraulics, continued as administrative supervisor for this project under D.I.C. 3-6616 for the Division of Industrial Cooperation of the Massachusetts Institute of Technology. Dr. James W. Daily, Associate Professor of Hydraulics, was in direct charge of all technical phases of the project. Dr. Kenneth C. Deemer was responsible for the design of the hydraulic and mechanical equipment and for the preparation and execution of the experimental program. Design and development of the electronic equipment was continued during this phase of the study by Mr. David L. Favin, Research Assistant. In addition, the following Research Assistants aided in the experimental program and in the evaluation of data: Mr. Wilbur L. Hankey, Mr. John D. Harms, and Mr. John P. Lawrence.

****

ABSTRACT

A project to investigate fluid friction and cavitation phenomena in unsteady motion by means of a special unsteady flow water tunnel of unconventional design has been under way in the Hydrodynamics Laboratory of the Massachusetts Institute of Technology under sponsorship of the ONR since 1948. Its objective is to obtain for transient flow conditions through conduits and around immersed bodies the same kinds of basic information that have been determined for steady flow cases. The initial phase of the program has involved the design and construction of a pilot model water tunnel to produce flow in which the basic motion is accelerating or decelerating, and the development of suitable instrumentation for measuring and recording unsteady velocities and pressures.

The tunnel is of the blow-down type and consists essentially of two tanks 20 in. in diameter and 6 ft. 8 in. long mounted vertically, one above the other, and connected by a tube, or working section, of one inch inside diameter. Flow from the upper tank passes through guide vanes and an entrance nozzle, through the one-inch tube which extends inside the lower tank, and through a quick-opening valve. High frequency response electronic cells were developed for measuring differential water pressures directly. These cells were employed in experiments to determine loss of head along the test section and for measuring the instantaneous average velocity.

The velocity and acceleration of the flow through the tube are governed by the difference in air pressure above the water surfaces in the upper and lower tanks. A servo control system has been designed and some components completed, but for initial experiments, control was effected by hand operation

of throttle valves to admit high-pressure air to the upper tank and to maintain constant pressure in the lower tank.

The loss of head due to fluid friction in turbulent flow was determined experimentally for steady and unsteady flow in a 1" diameter smooth brass tube 9 ft. long. Measurements were made in a section where the boundary layer was fully developed. Unsteady flow runs were made with average velocities of 15 to 72 ft/sec and average accelerations from zero to 35 ft/sec^2.

Results of the experiments to date indicate that there is no appreciable difference between the friction factors referred to the instantaneous velocity for steady and unsteady flow as long as the rate of acceleration is constant or changes slowly. For sudden impulses from steady flow to accelerated flow, the measured values of the wall shearing stress, τ_o, are below those for steady flow at the same instantaneous average velocities. This indicates a change in the distribution of internal shear stresses and velocity distribution from the steady flow distributions at the same velocity. These results for sudden impulses, although obtained consistently, are considered tentative pending accumulation of additional test data.

The experimental work performed to date is but the initial phase of a long-range program and marks the initial successful operation of the tunnel and instrumentation. The long-range program is to construct a much larger tunnel with a test section of sufficient diameter to permit studies on submerged bodies for cavitation and hydrodynamic forces in unsteady flow. Work will be continued on the present tunnel, not only with the hope of obtaining more fundamental knowledge in hydromechanics of unsteady flow, but with the aim of developing an adequate control system and determining optimum design data for the larger tunnel.

TABLE OF CONTENTS

LIST OF ILLUSTRATIONS

I INTRODUCTION

All known water tunnels constructed prior to the one described herein have been for steady flow. While they have contributed tremendously to the knowledge of steady flow fluid friction and cavitation phenomena (1), they have not been capable of yielding comparable information for unsteady flow. In 1948 the basic features of a special "unsteady flow water tunnel" analogous in some ways to the blow-down tunnels for air were conceived and analyzed at the Hydrodynamics Laboratory of the Massachusetts Institute of Technology. Under the sponsorship of the Office of Naval Research, a project to build a water tunnel of unconventional design which would be devoted primarily to studies of unsteady flow was initiated. The program was also to include the development of instruments for measuring instantaneous velocities and pressures.

The overall objectives of the program, as set forth in an earlier report (2), are to investigate and correlate the characteristics of fluid friction and cavitation for steady and unsteady flow through conduits and past submerged bodies. This is to include an investigation of the characteristics of boundary layer flow and an attempt to establish whether the boundary flow and its relation to fluid friction differ from the laws established for steady flow. The inception and growth of cavitation as affected by local acceleration and by presence of dissolved gases is to be investigated also.

The design of the tunnel and experiences in developing instruments were described in an earlier report. Design considerations led to the construction of a pilot model blow-down type tunnel having a 1" diameter test section. Tunnel costs increase rapidly with size, but the instrumentation for a small tunnel can be carried over to a larger one with little alteration. This report covers the first period of operation of the tunnel and contains an account of experimental studies of fluid friction due to accelerated flow in a conduit. An electronic differential cell is described which is used to "instantaneously" measure average velocities and pressure drops.

The primary objective of the present investigation is to employ the tunnel to determine whether or not the presence of an acceleration affects the wall shear stress in flow through a circular conduit of uniform diameter. It was first proposed to obtain overall effects, and, if these were pronounced, to then conduct more detailed experiments.

Only fully developed turbulent flow at distances of not less than 60 diameters from the entrance to the test section were considered in this study. Steady flow runs were made with Reynolds numbers from 75,000 to 750,000 (average velocities about 9 to 85 ft/sec). Unsteady flow runs were made with average velocities from about 15 to 75 ft/sec and average accelerations from zero to about 35 ft/sec^2.

A discussion of some features of unsteady flow in tubes is presented in Section II which follows. The experimental equipment and procedures are described in Section III and in the Appendix. The results of test measurements and discussion of them are given in Section IV.

II SOME FEATURES OF UNSTEADY UNIFORM FLOW IN TUBES

A. Acceleration in Steady vs Unsteady Fluid Motions

Fluid motion is classified as steady or unsteady, uniform or non-uniform. Unsteadiness means a variation of the local velocity with time. Non-uniformity means a variation of the local velocity from point to point along a streamline. At the entrance to a tube from a reservoir, non-uniform flow is obtained as the boundary layer thickness grows radially. Uniform flow results after some distance when the velocity profile becomes fully developed by the radial convergence of the boundary layer.

The study of unsteady motion is one of the approaches for examining the effects of acceleration. A virtue of using unsteady motion lies in the ability to cause local acceleration independently of velocity and boundary geometry. Only by this method can the simple case of acceleration of a uniform flow be studied. With steady motion, acceleration is possible only with non-uniform flows. In these cases, convective acceleration of a fluid element as it moves through the fluid-filled space depends upon the magnitude and direction of the velocity and the shape of the boundary.

There have been previous studies of accelerated flow in tubes. First, the steady non-uniform flow at the entrance to a tube from a reservoir, wherein the circular core is accelerated as the boundary layer grows along the tube, has been subject to several investigations. These include the early study by Boussinesq (4) in 1890 and by Schiller (5) and later by Langhaar (6), and others. Second, cases of unsteady uniform flow have been examined including analytical studies of oscillatory motions in U-tubes and long straight tubes (8), (9), and (10), and laminar flow in smooth round tubes (11). As already noted, the unsteady measurements reported here are for uniform turbulent motion in a smooth round tube.

B. Kind of Flow Under Investigation

As a basis for examining the kind of flow to be expected, use is made of the boundary-layer equation developed by Prandtl (12) and Von Karman (3) which is obtained by equating the rate of change of momentum in the boundary layer to the sum of the pressure drop and shear stress forces.

For simplicity, consider the case of two-dimensional flow between parallel flat plates described by the diagrams below. The momentum equation, for flow with a pressure gradient in the direction of motion only, can be written

$$\int_0^h \rho \frac{du}{dt}\, dy + \frac{d}{dx}\int_0^h \rho u^2 dy - \rho u_1 \int_0^h \frac{du}{dx}\, dy = -h\frac{dp}{dx} - \tau_o$$

where x is distance along a plate, y is distance normal to a plate, u_1 is the velocity of the flow at y = h, u is the local velocity within the boundary

layer at a distance y from one bounding plate, h is half the distance between the two plates (and is independent of time and distance x), p is local pressure intensity, and τ_o is local boundary shear stress. This equation is customarily applied to turbulent motion by replacing u with $\bar{u}$, the temporal mean velocity.

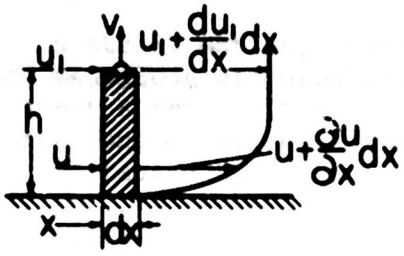

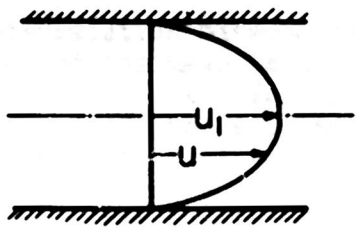

This equation indicates a relationship between pressure gradients, velocity gradients, local acceleration, convective acceleration, and wall shear stress. It is to be noted that this equation does not account for rotational components or for a pressure gradient normal to the wall. Rotational components normal to the wall are considered negligible in the experimental setup because appropriate measures have been taken to eliminate such flow at the entrance to the test tube. In general, $\frac{dp}{dy}$ as well as $\frac{dp}{dx} \neq 0$, and the first term on the right-hand side of Equation [1] could be written

$$\int_0^h \frac{dp}{dx}\, dy$$

This means, however, that if $\frac{dp}{dx} \neq 0$, there is a normal acceleration, i.e., curvilinear flow. Acceleration normal to the wall is known to occur in this region of boundary layer development near the entrance to a tube; on the other hand, sustained flow curvature in a long duct is improbable, and from continuity considerations, the normal velocity component becomes a smaller and smaller percentage of the longitudinal component as the boundary layer becomes fully developed. The reduced curvature must result in reduced normal acceleration, and hence in negligible pressure gradients normal to the wall. This argument, of course, assumes no compressibility effects such as might lead to standing waves.

The work reported here is based on measurements 60 diameters and beyond the entrance to the tube where fully-developed flow can be reasonably expected; hence, dp/dy is taken as zero. In this zone, the flow is uniform, and at any instant of time there is no change in velocity of a filament along x; hence, the second and third terms of the left-hand side of Equation [1] drop out. Also, at any instant of time, dp/dx is a constant in this zone. The remaining term on the left side represents the acceleration. For any distribution of acceleration over the cross-section, this integral is equal to the product of the average acceleration and the cross-sectional area, since

$$\bar{a} = \frac{\partial v}{\partial t} = \frac{1}{A}\frac{\partial Q}{\partial t} = \frac{1}{A}\frac{\partial}{\partial t}\int_0^A u\,dA = \frac{1}{A}\int_0^A \frac{\partial u}{\partial t}\,dA \quad \text{and} \quad A = h$$

for the two-dimensional flow which Equation [1] represents.

Equation [1] now has been reduced to the very fundamental Newtonian expression $\rho h \bar{a} = \tau_0 \ell + \Delta p \ell$, an expression which might have been written directly. The development through application of the momentum relation, however, serves to point out that τ_0 may no longer be the τ_0 of steady velocity flow.

C. Wall Shear Stress and the Distribution of Mean Velocities

In steady motion, there is a definite interrelation between the distribution and magnitude of turbulence, the distribution of the mean velocity, and the wall shear stress. Thus it is logical to infer that for the fully developed region under consideration, a modification of the shape of the velocity profile that might be caused by an acceleration would alter the shear stress and vice-versa. Clearly, it is desirable to study both the kinematics and dynamics of unsteady motions in order to have a complete picture of the acceleration effects. In the present study, the direct measurement of the velocity distribution was not practical because of the small size of the 1" diameter tube. Consequently, it was possible only to measure the change in pressure gradient, calculate the wall shear and infer the probable change in velocity distribution.

It is interesting to consider qualitatively the possible effects of acceleration on the relationship between shear stress and velocity distribution with turbulent motion. In steady uniform flow in a conduit, the linearly distributed mean shear stress is developed as a consequence of a particular distribution of velocity and turbulence. The turbulence pattern in the central portion of the stream is maintained by the continuous generation and diffusion of turbulent eddies due to high shear forces in a narrow zone near the solid boundary. In fact, this turbulence pattern is developed by a spreading of the boundary influence from all sides until a convergence at the center gives the uniform condition. Thus, the establishment of uniform flow is dependent upon a time and space factor. At conduit transitions, a new regime of uniform flow is not established immediately but appears after some suitable transition distance. An example is in a contraction where the magnitudes of the velocity fluctuations are only slightly affected in passing through the transition. One might conclude that if an established uniform motion is accelerated from one velocity to another, some transition time may be necessary before a new established condition is effected. In other words, a time lag may occur to allow the turbulent eddy generating mechanism to adjust to new conditions and to reinforce and rearrange the turbulent pattern. With the existence of such a time lag, the velocity distribution and hence the wall shear stress may not be the same during the transition period as for steady flow at the same instantaneous velocity. Any difference would depend upon the magnitude of the time lag and the absolute time increment that such a flow readjustment takes. Experiments should indicate whether or not appreciable differences exist.

Next it is interesting to consider the possible effects of acceleration on the mean local velocity distribution and the wall shear that might be encountered during this transition period. Kinematically there are several possibilities.

Figure 1 shows a steady velocity profile in (a) and three profiles (b), (c), and (d) representing alternate assumptions concerning the effect of an acceleration acting for a time Δt.

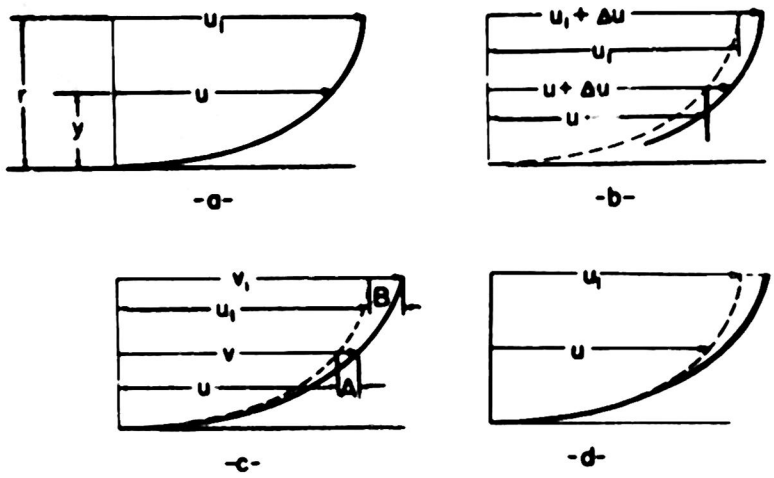

Fig. 1: Profile Changes Due to Acceleration

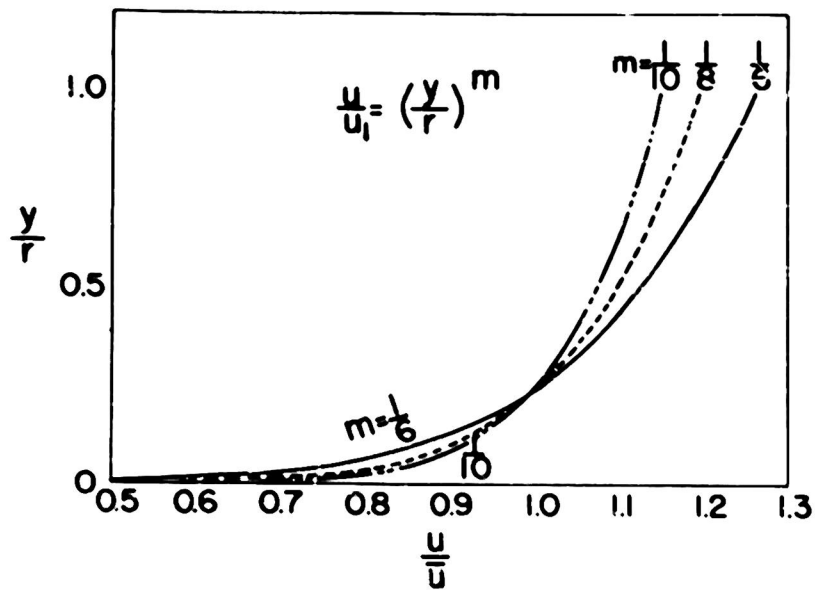

Fig. 2: Exponential Type Velocity Profiles

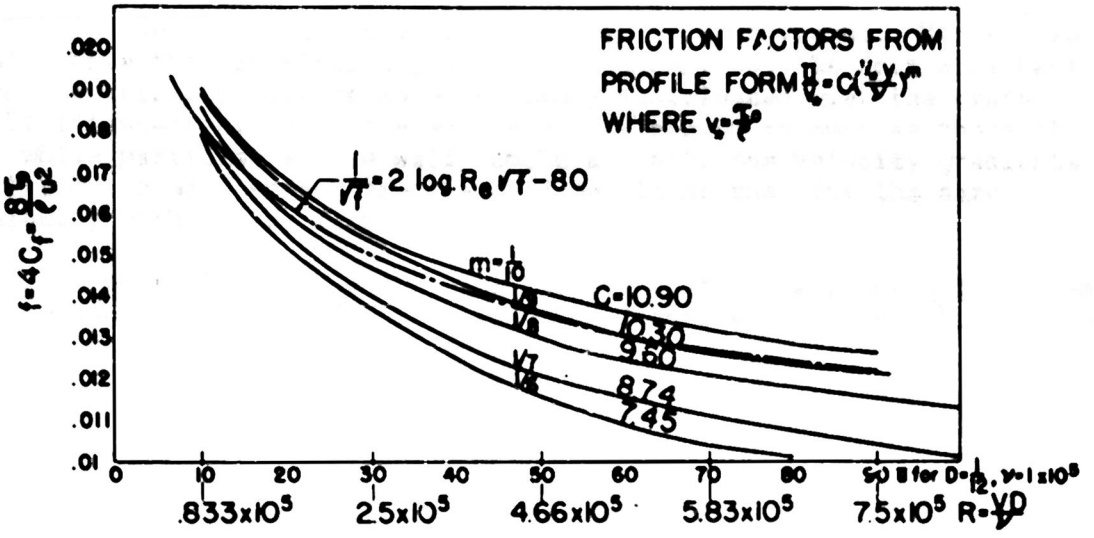

Fig. 3: Friction Factors for Assumed Exponential Velocity Distributions

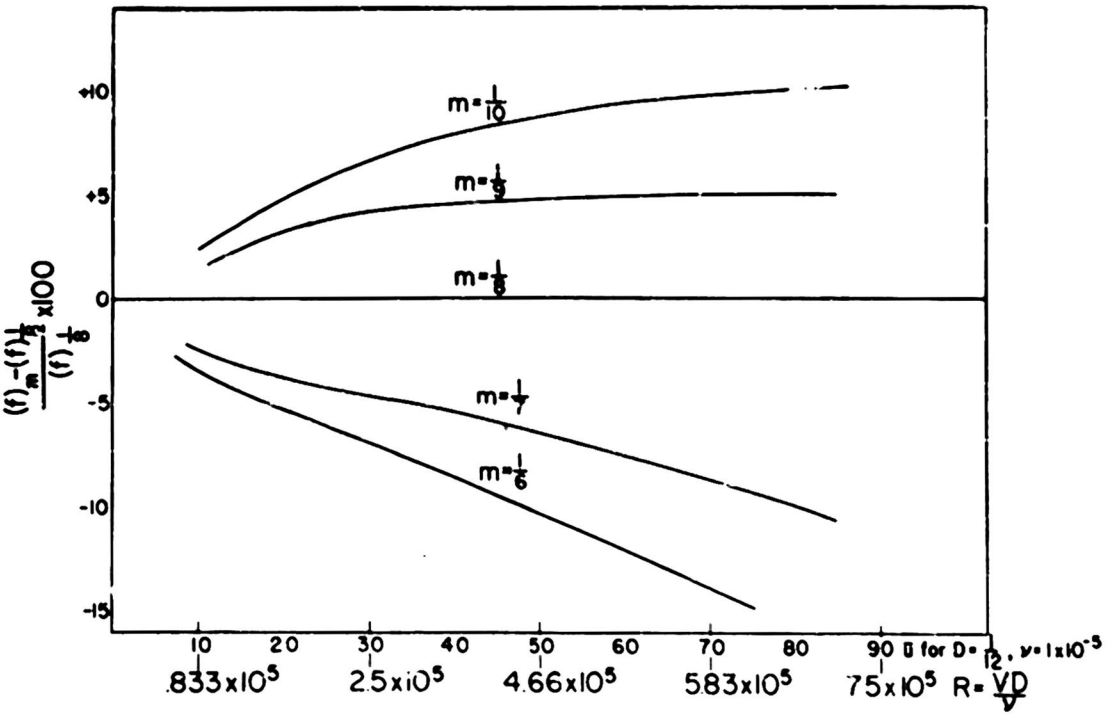

Fig. 4: Percentage Change in Friction Factor for Change in Velocity Distribution

In (b) each filament is accelerated by the same amount. Hence, profile (b) will have the identical shape as that in (a), but the form will have changed and the velocity will be more uniformly distributed over the cross section. If filaments close to the wall are accelerated as much as those at the center while particles at the wall remain at rest, the velocity gradients at the wall and the wall shear stress should be higher than for the same average velocity with steady flow.

The profile in (c) has the same form as that in (a), but not the same shape. For example, if an exponential equation describes profile (a), the same equation describes profile (c).

Let profile (a) be $\frac{u}{u_1} = \left(\frac{y}{r}\right)^m$ at time t

Let profile (b) be $\frac{v}{v_1} = \left(\frac{y}{r}\right)^m$ at time $t + \Delta t$

$v_1 = u_1 + B$

$v = u + A$

$$\frac{u + A}{u_1 + B} = \left(\frac{y}{r}\right)^m = \left(\frac{u}{u_1}\right)$$

$$u_1 A = uB$$

$$\frac{u}{u_1} = \frac{A}{B} = \left(\frac{y}{r}\right)^m$$

Thus, in this case, the acceleration is distributed over the cross section in the same manner as the mean local velocity.

As a third case, let it be assumed that the central portion is accelerated more than in the second case, causing the velocity profile to become more "peaked" with subsequent relatively lower velocity gradients at the wall. This case is illustrated by Figure 1 (d) wherein the profile near the wall at $(t + \Delta t)$ is shown approximately coincident with that at time (t) while the average velocity has increased. In this case, neither the shape nor the form of the velocity distribution curve has been preserved, and during acceleration τ corresponding to an instantaneous average velocity would appear to be less than for steady flow at the same average velocity.

It is not easy to decide a priori which of these three possibilities will exist. A time lag could conceivably lead to either of the two extremes represented by (b) and (d), whereas if turbulence generation and diffusion is rapid enough, case (c) would be realized.

D. Estimates of the Effect of Velocity Distribution Change on Shear Stress

It is interesting to establish a measure of the deviation of the velocity distribution-shear stress relation during transient conditions from that for the equivalent steady flow. As already noted, this can be done by comparing experimentally determined shear stresses. A simple estimate of the magnitude of the effect can be obtained using the power law velocity distribution

equation

$$\frac{u}{v_*} = C\left(\frac{yv_*}{\nu}\right)^m$$

If m is taken as 1/7 and C as 8.74, the expression is valid in the Reynolds number range from 3000 to 100,000 and for higher ranges m is taken as 1/8, 1/9, etc. In Figure 3, pipe friction factor curves calculated for several values of m and C are compared with the Karman-Prandtl logarithmic pipe friction factor curve over the range of Reynolds numbers considered in this report. Figure 2 shows the velocity profiles represented by m values from 1/6 to 1/10.

If it is now assumed that the velocity profile (at least in the neighborhood of the wall) retains an exponential form during an acceleration and that only the constant and exponent change, predictions as to change in form can be made from observations of change in wall shear stress. Figure 4 is a plot of percentage change in pipe friction factor corresponding to deviations in the form of the velocity distribution profile from that described by m = 1/8 and C = 9.60 which is arbitrarily taken as reference base. For example, it can be seen from Figure 4 that at a velocity of 50 ft/sec., a gain in the friction factor of 4-1/2% over the friction factor corresponding to steady flow at the same velocity would indicate a steepening of the profile from the 1/8th to the 1/9th exponential; on the other hand, a decrease of about 6-1/2% in f would indicate the less steep profile described by the 1/7th exponential.

It is not proposed here that these exponential laws actually represent the velocity distributions in accelerated flow. They do, however, serve as a means of qualitatively expressing a change in form of the velocity distribution profile corresponding to a change in shear stress.

III EXPERIMENTAL EQUIPMENT AND PROCEDURES

A. The Unsteady Flow Water Tunnel

The design considerations and construction details of the tunnel are set forth in Reference #2. The primary elements consist of two 20" diameter by 6' -8" long tanks connected by a 1" diameter test section as shown in Figures 6 and 7. Eight piezometer taps are located along the test section at distances of 0, 9, 21, 33, 45, 60, 79.5 and 99 diameters (inches) from the entrance as shown in Figure 7.

Driving force is supplied by regulating the air pressure above the two water surfaces. An electronic control system is being developed for the tunnel, but the work reported herein was carried out by hand operation of throttle valves to regulate air pressures in the two main tanks.

B. Instrumentation

For this investigation of loss of head due to unsteady flow in conduits, three variables are to be determined.

1. Instantaneous head loss along the tube
2. Instantaneous velocity
3. Instantaneous acceleration

In steady flow measurements, accuracy is of prime importance and time is not ordinarily considered a major factor. In unsteady flow measurements, however, it is essential that all variables be measured at the same instant; hence, it becomes imperative to have high frequency response indicators and recorders.

Diaphragm type pressure cells, incorporating several types of electronic measuring principles, have been designed and employed in numerous investigations. The diaphragm cell exhibits high frequency response and requires but a small amount of fluid to actuate it. In general, diaphragm type transducers cannot be relied upon to have an error of much less than 1% of full scale, and this sacrifice in accuracy is justifiable only when the high frequency response characteristic of this type of transducer is required. When measuring total pressures, a 1% error may often be completely satisfactory, but when a pressure difference between two points is desired, it is quite possible that two such errors in opposite directions in each of two gages may be equivalent to an error of many times the magnitude of the actual differential pressure. To avoid such difficulties, it was necessary to develop a gage which would measure rapidly changing differential water pressures directly.

A pressure cell was developed which measures differential pressures independently of total pressures. Four interchangeable diaphragms and three interchangeable electronic elements permit measurement of differential pressures from less than 0.01 to more than 200 ft. of water. Total pressures employed have been up to 200 psi. The natural frequency of the cells with air on both sides is from 500 cps for the softest diaphragm, to 6200 cps for the stiffest one. The

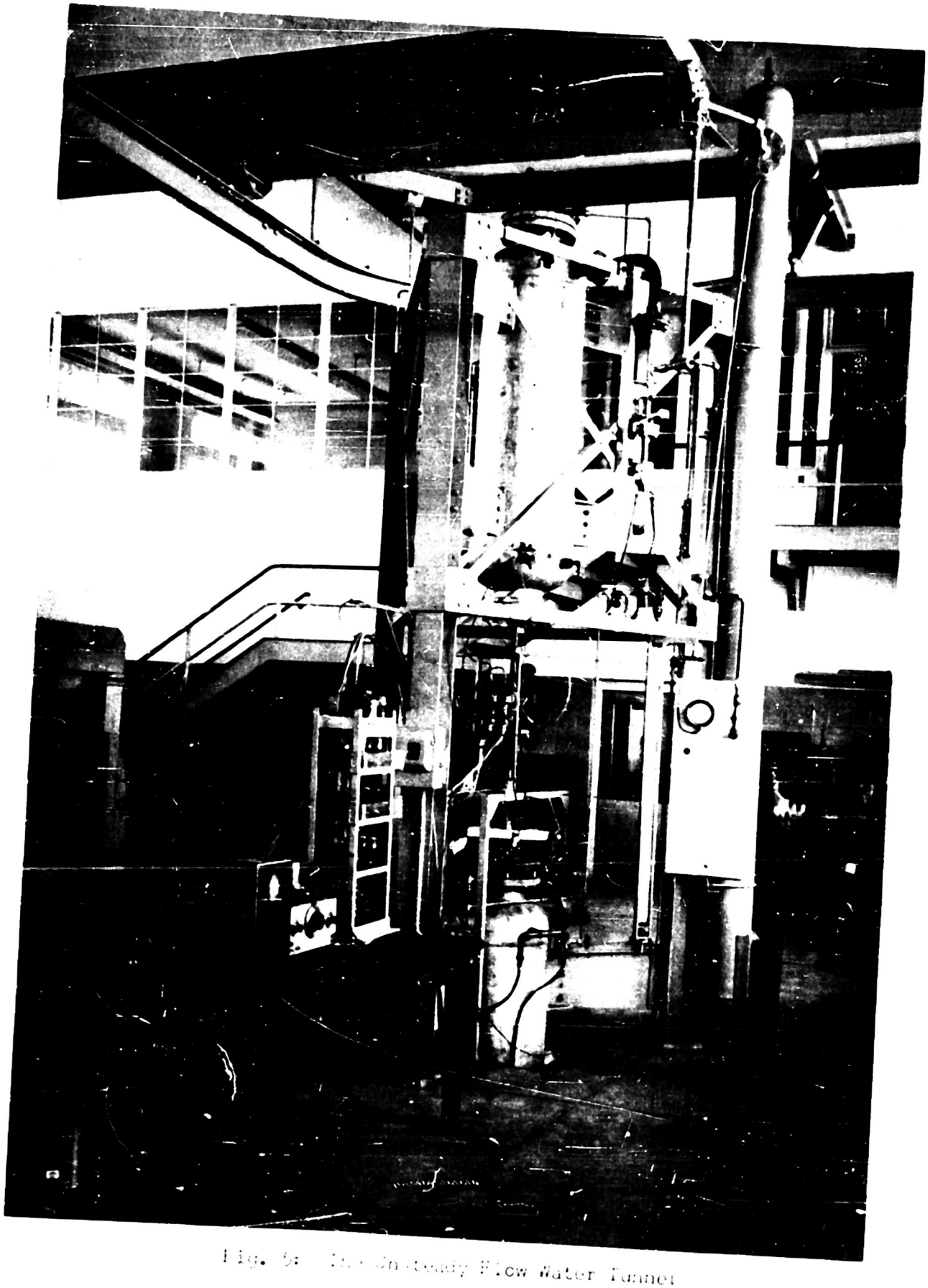

Fig. 5: [illegible] Unsteady Flow Water Tunnel

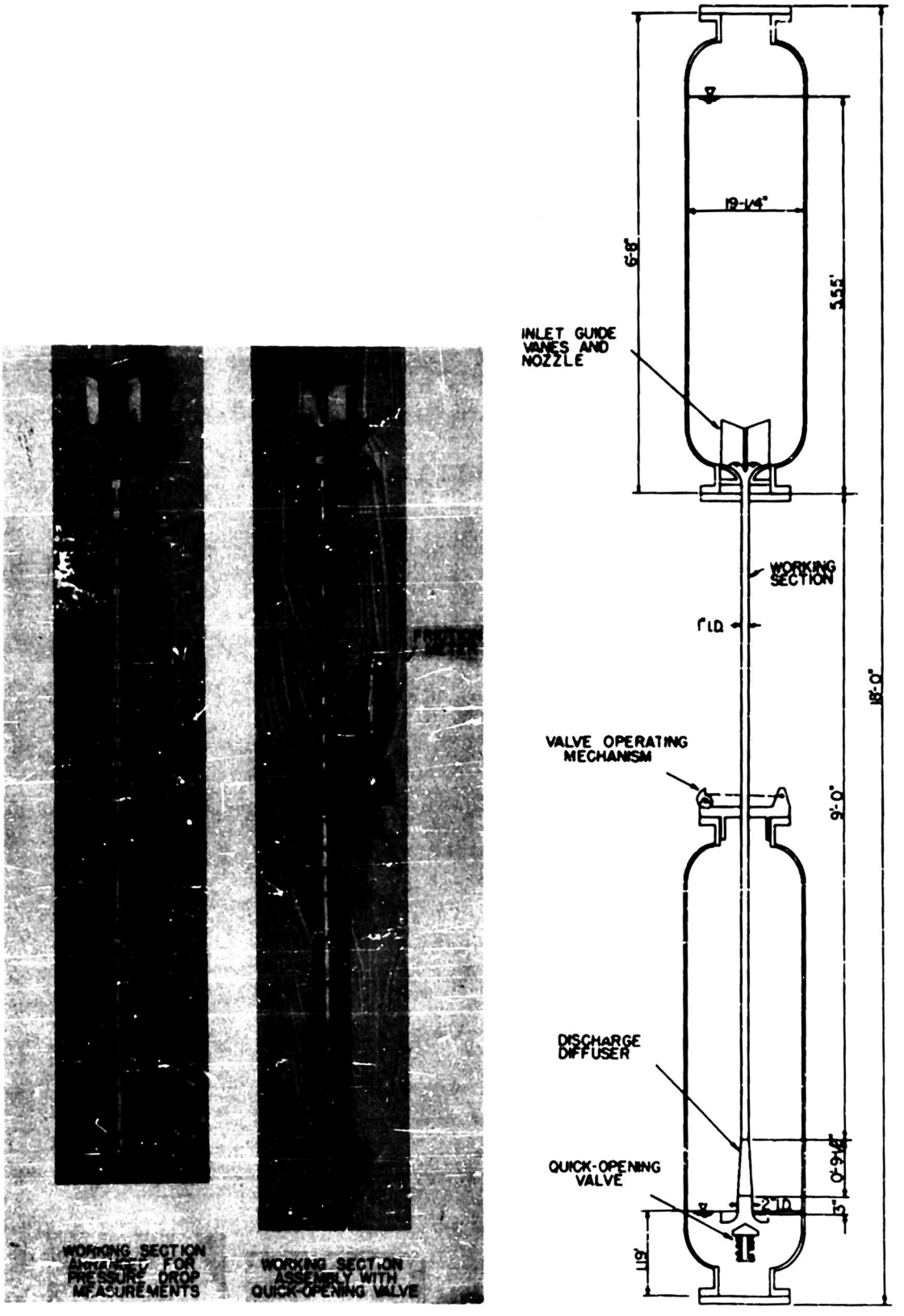

Fig. 6: Schematic Section of Pilot Tunnel Circuit

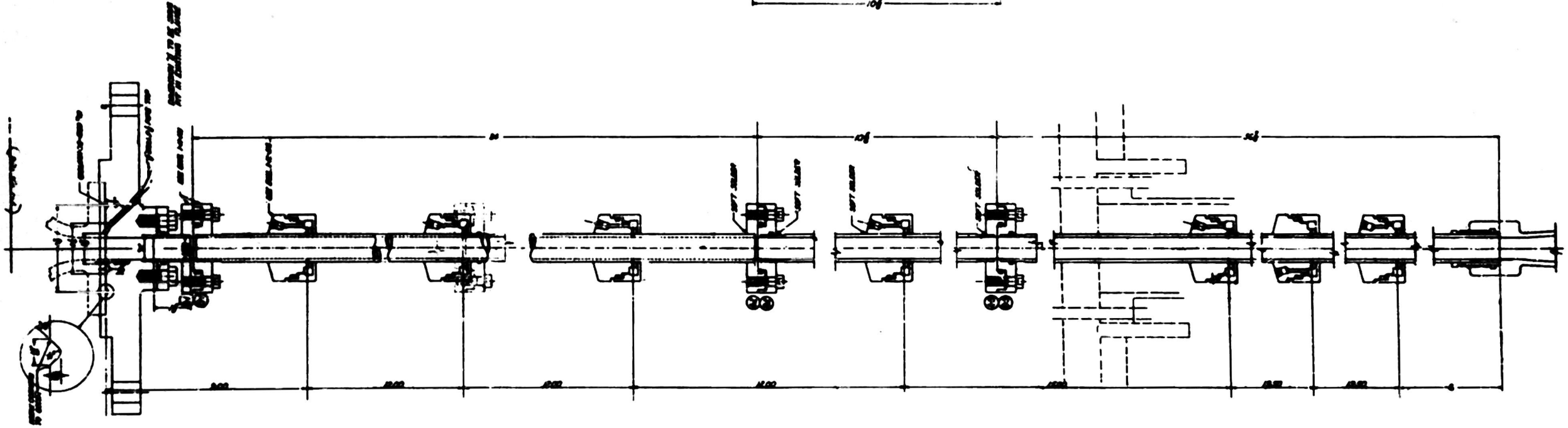

Fig. 7 Pilot Tunnel Test Section Assembly

overall frequency response for the cells as applied in this study (including water filled lead lines, piezometer taps, amplifiers, and galvanometers) has been found to be at least 160 cpc to 300 cps for three types of diaphragms used for measuring rapidly changing differential pressures. The softest diaphragm was employed only for measuring tank levels. A complete description of the differential pressure cell developed for this investigation is to be found in the Appendix.

The average instantaneous velocity is measured by utilizing the inlet nozzle as a venturi section and accounting for the acceleration head, and a check is provided by recording the water level in the tanks as a function of time. Differential pressure cells are employed in both cases. In the former, of course, the cell measures the differential head at the venturi. In the latter, the cell measures the difference between the pressure in the bottom of a tank and the pressure in the air section, i.e. the water level. An analysis of the acceleration effect on venturi measurements is given in D of this section.

Acceleration is not measured directly but is calculated from the slope of the instantaneous velocity-time record. It would be possible to employ an electronic square-rooter and differential analyzer to obtain this record directly from the venturi differential head.

The differential heads representing velocity and pressure drop along the tube are recorded on a Hathaway-type S-8 B Oscillograph. Galvanometers used in this investigation have a frequency response of 750 cps. Sample records are shown to a reduced scale in Figure 8. Two traces represent tank level, three represent head loss along the test section, and one is the velocity indicated by the throat venturi. Time lines appear on the chart at intervals of 0.01 second with each 0.1 second appearing darker than the others. In Figure 8, the time lines were lost in the reduction and the one-second lines were ruled in with a pen for reference.

C. Test Procedures

1. Operation of Tunnel for Steady and Unsteady Flow Runs:

In essence, a run is made by blowing water down from the upper tank to the lower tank through the 1" diameter test section and obtaining measurements of velocity, acceleration, and pressure drops along the test section. The methods of making these measurements are described later in this section.

To prepare for a run, water is forced from the lower to the upper tank through the test section by opening the foot valve and supplying air pressure to the space above the water surface in the lower tank. When the proper amount of water has flowed into the upper tank, the foot valve is closed and the air pressure in the lower tank reduced to about 30 to 40 psi, depending on the maximum velocity of the test to be made. This pressure in the lower tank is held to assure positive pressure in the lead lines to the pressure gages.

Air is then admitted to the upper tank above the water surface by a 1" hand throttle gate valve to a value about 5 or 10 psi greater than that required to produce a predetermined steady velocity in the test section with the positive pressure in the lower tank as noted above.

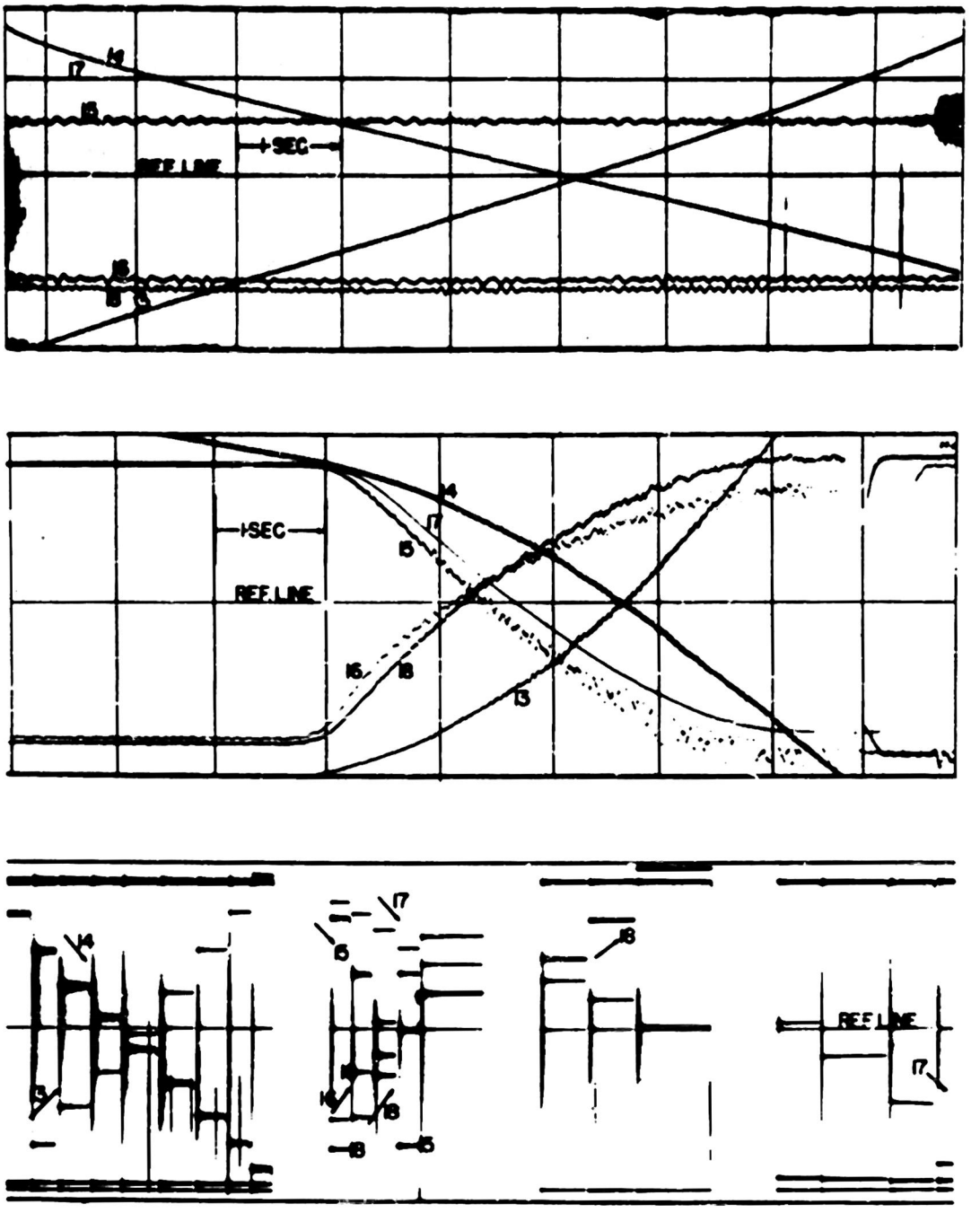

Fig. 8: Sample 10" wide Oscillograph Chart Records

At a signal from one operator, the foot valve is opened and the water begins to flow. For steady flow runs, pressure in the lower tank is held constant by bleeding out through a hand throttle valve; pressure in the upper tank is also maintained at a constant value by bleeding in air from the high pressure air receiver through another hand throttle valve. Once the flow is established, very little adjustment is needed on either of these valves to maintain constant velocity in the test section. Both pressures are noted on Bourdon-type pressure gages. Actually, the pressure maintained in the top tank is not the air pressure but is the pressure of water head plus air pressure just above the inlet nozzle.

Although the water level in the upper tank falls about three feet during a run, data is only recorded during about 0.6 feet of this fall. Approximately 1.75 feet is utilized to establish desired test pressures, 0.6 feet is for running, and the balance for turning off gages and stopping the flow.

As soon as the flow is established and danger of water hammer transients damaging the differential pressure gages is over, the gages are opened to position for measuring. When the running zone is reached, the recording oscillograph is turned on by remote control (hand) and the data is recorded.

When the water level has passed the running zone, the pressure gages are shut off (again to avoid water hammer effects) and the foot valve is closed. The water is then returned to the upper tank for another run or for calibrations, which are described in later paragraphs in this section.

Unsteady flow runs differ from the steady flow runs described above only in the method of operating the upper tank inlet air throttle valve. In these runs, the running zone is approached with a fairly low steady velocity. In the running zone, this hand throttle valve is opened rapidly and the resulting impulse accelerates the water through the test section. When a record is desired which will begin and end with steady velocities, the pressure is eased off about half-way through the running zone.

A set of tests usually consists of gage calibrations alternated with runs, and the usual practice is to stretch this to three runs between each set of calibrations after the first few cycles. About four or five minutes are required to prepare for and make a run, while the actual duration of a run is only about 20 or 30 seconds, and as little as 3 or 4 seconds of this may be in the running zone. Calibrations between runs require about ten minutes.

2. Operation of Differential Pressure Cells

Each differential pressure gage measuring head loss along the tube is fitted with a Christmas tree" loop, consisting of a valve (#4) at the inlet to the high-pressure side of the diaphragm, another at the inlet to the low-pressure side (#2), a by-pass valve (#3), and a bleed valve (#1). The purpose of the first three valves is to prevent shock arising from opening and closing the foot valve at the test section from reaching the diaphragm. The fourth is for calibrating. Such shocks arising from accidental failure to open the by-pass have been observed to overstress and dish diaphragms and on one occasion to completely rupture one. Figure 9 shows a gage with its valving.

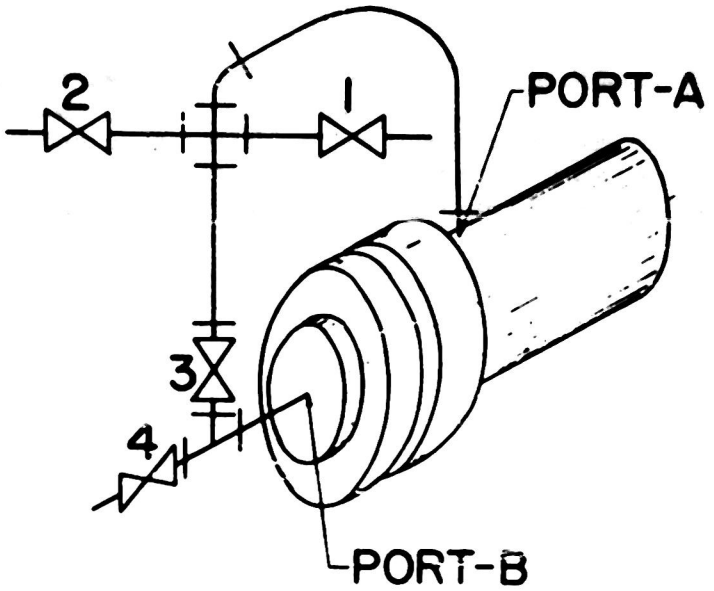

Fig. 9: Christmas Tree Valving on Differential Pressure Cell

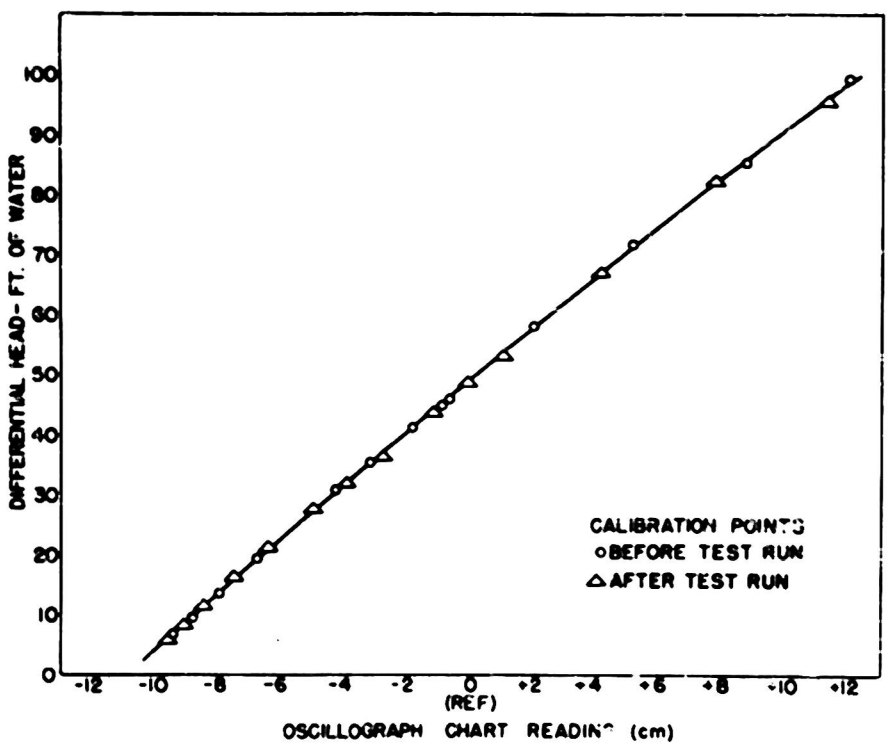

Fig. 10: Typical Calibration Curve for Differential Pressure Cell

When a run is to be made, the by-pass valve is opened and the two inlet valves closed. As soon as the quick-opening foot valve at the bottom of the test section is opened, the gage inlet valves are opened and the by-pass is closed in that order. This operation occurs before the running section is reached. As soon as the water has passed the section where velocities are measured, the Christmas tree valves are operated in reverse order, i.e. the by-pass is opened and the inlet valves are closed. When all gages have thus been positioned, the foot valve is closed to end the run.

3. Calibration of Differential Pressure Cells

The differential pressure gages are calibrated frequently during each test period. The usual practice is to calibrate the gages, make one blow down run, and to then repeat the cycle until the completion of the test period which normally is three to four hours long. Each calibration period normally requires about 10 minutes, and the gages are not removed from their positions on the rack.

Referring again to Figure 9, valves #1 and #4 are opened and #2 and #3 are closed. This allows pressure to be applied to the upper side of the diaphragm while the lower side is vented. For convenience, a short length of tubing is attached to valve #1, which terminates in a small well at the zero position of the water column scale on the upper tank; consequently, the lower side of the diaphragm is not at atmospheric pressure. The net pressure on the gage is now the level of water in the upper tank indicated on the water column, plus the air pressure above the water surface.

A water manometer and a mercury manometer are manifolded to measure the air pressure above the water surface in the upper tank. Air is now fed into the upper tank through a small needle valve. At somewhat random increments of pressure shown on one of the two manometers (depending on the magnitude of the pressure), the needle valve is closed and one operator gives a signal to take readings. At this time, a short burst is run on the recording oscillograph, the water column level is read, and the appropriate reading is made of the air pressure in the upper tank. Readings are recorded on a data sheet. A typical calibration chart record is shown in Figure 8 c.

D. Computational Procedure

Only those test runs are considered where the preceding and subsequent calibrations have not shifted. A typical calibration curve is shown in Figure 10. Such curves are plotted by measuring the distance of the bursts from the reference line in Figure 8 c and correlating each burst with a data sheet value of known differential pressure applied to the cell. The calibration curves show the position of a trace on the oscillograph chart versus differential pressure. By scaling a trace on a test run and consulting the proper calibration curve, one obtains plots of differential pressure versus time.

A constant velocity test run is shown in Figure 8 a. Velocity is obtained from the venturi differential cell trace 17 and is checked against the fall in tank level given by traces 13 and 14. Traces 15, 16, and 18 represent pressure drops from 60 to 99 diameters from the entrance to the test section respectively. Head loss in feet per foot for these steady flow runs is averaged from the last three traces and friction factors are calculated using these head losses and the velocity given by the venturi meter and level gages.

In general, computation of unsteady flow runs follows that for steady runs as far as obtaining values of velocity and head losses from the traces. However, certain variations in the procedure are necessary.

Design of the tunnel included a pressure tap at the throat of the inlet nozzle in the form of an opening 0.010" wide completely around the periphery of the test section (see Figure 7). This tap permits direct employment of the nozzle as a venturi for steady flow. For unsteady flow, however, the pressure drop across the nozzle indicates both the change in velocity head and the inertia force due to the local acceleration of the fluid through the nozzle.

The extra pressure due to this inertia effect is small, and so was determined approximately by using a value calculated for irrotational motion through a two-dimensional nozzle having the same boundary geometry. This calculated value was 0.18 $\frac{\partial v_t}{\partial t}$, where v_t is the instantaneous average velocity in the test section. The maximum correction was of the order of 2% for the lowest velocities and highest accelerations covered by the tests and was less than 1% for the maximum velocities at the highest accelerations.

In computing unsteady flow runs, the velocity-time curve is first plotted to a scale which allows first differences of velocity to be calculated to yield acceleration. The slope of the velocity curve is obtained both by numerical differences and tangents. These accelerations are then used with the above equation to correct the velocities for the inertia effect, and new velocity and acceleration curves are plotted against time.

The area under the adjusted velocity curve is now calculated and compared to the change in level indicated by the level gages over several increments of time; however, while this affords a check, the level indications are less reliable than the velocity obtained from the venturi. The acceleration curve is now computed more precisely than for the first trial mentioned above, and the area under the curve is checked against velocity change for about 1/2 second intervals.

The measured pressure drop or "head loss" during the unsteady runs is reduced to feet per foot and plotted versus the time scale of the run. The head loss due to friction in steady flow for the instantaneous velocities computed from the constant velocity runs is also plotted on this time scale in feet per foot. Finally, the acceleration head in feet per foot is added to the steady state friction head loss ordinates to permit comparison of the pressure drop computed in this manner with the measured pressure drop or unsteady flow "head loss." (Note that in Figures 12, 13, and 14 in Section IV, crosses are placed at 0.1 second intervals to designate the computed unsteady head loss. The measured head loss curve is broken to accommodate these crosses because the values fall so close to each other).

In addition to differences in methods of computing steady and unsteady flow runs, there is a difference in the data used. As noted on page 17, the average head loss indication from three spans was used to obtain the steady flow friction factors. When the calibration shifted for any one pressure cell during a run, the readings from that gage were not included in the calculations. It would be extremely difficult to exactly duplicate unsteady flow runs by hand operation of the throttle valves and thereby obtain data which could be averaged. For this reason, a pattern of unsteady flow runs was adopted which provided a check on the reliability of the recorded differential pressures.

Unsteady flow runs were made by accelerating the flow from one steady velocity to a higher one. The constant velocity portions of these runs provided

an opportunity to check the head loss readings of each pressure cell with the head loss data obtained from more extensive constant velocity tests. Moreover, completely steady flow runs were sandwiched between the unsteady flow runs to provide an additional check.

It was observed that this steady flow data obtained during the unsteady flow tests gave a random scattering of points about the smooth pipe curve similar to the scattering shown in Figure 11. It was noted, however, that the combination of piezometer taps, lead lines, pressure cell, and amplification system on the span from 79.5 to 99 diameters from the entrance showed considerably less deviation from the mean value (the smooth pipe curve) than was found on either of the other spans (60 to 99 diameters and 60 to 79.5 diameters). For this reason, only the measured head loss data from the span at 79.5 to 99 diameters from the entrance was plotted.

E. Experimental and Computational Precision

Precision of results from the experimental work depends on the accuracy, both as to magnitude and time, with which differential pressures are recorded on the oscillograph chart and on the accuracy with which these records can be reduced to numerical data.

1. Pressure Indications:

It has been found (see page 45, Appendix) that the differential pressure measuring systems respond to frequencies of at least 160 cps which indicates there is no appreciable time lag between a pressure change and its detection. Hysteresis plays a minor role inasmuch as diaphragm deflections increase continuously during a run (except for small pressure fluctuations about the mean). The practice of making calibrations before and after each run, and of computing only those runs where these two calibrations are the same, increases the reliability of recorded pressure values.

A large portion of the calibration shifting is due to the electronic equipment. It has been found that the output voltage from the oscillator which energizes the pressure cells (see Appendix) is subject to fluctuations. These fluctuations are primarily due to variations in line voltage and to vibrations caused when heavy trucks pass the laboratory. Although the absolute variation is small, the amplification of the signal from the pressure cells is sufficient to make the shifts of zero position on the oscillograph chart noticeable. The practice of using only the runs where the calibrations remain constant minimizes this error.

2. Conversion of Data from Oscillograph Charts:

Diaphragms and transformers are so selected and amplification of the output signals so regulated, that the ranges of differential pressures covered by a pressure cell during a test run will extend over approximately 20 cm. on the recording chart. Errors arise in scaling the calibration charts shown in Figure 8 c and in reducing the deflections on the test charts (Figures 8 a and 8 b) to differential pressures.

(a) Errors in Obtaining Data from Calibration Charts: Three observers have found they read the distance of the same calibration marks from the chart reference line within 0.3 mm. Smooth calibration curves are drawn

through the two sets of calibration points for each run as shown in Figure 10 and errors in reading chart values are thereby reduced.

(b) Errors in Obtaining Data from Test Run Charts: Due to the large amplitude of differential pressure fluctuations about a mean value as indicated in Figures 8 a and 8 b, the three observers read the mean value within 1.0 mm at full scale and within .5 mm at 1/4 to 1/5 of full scale deflection. Although the absolute value of the fluctuations, which may be due to turbulence, increases with velocity, the amplification of a signal to give full chart deflection for different ranges of differential pressures makes the fluctuations more or less a function of chart deflection.

The overall error in converting data from the oscillograph charts to numerical data may be as high as 1.3 mm in 20 cm. at full chart deflection and 0.8 mm at small deflections. At full scale this is equivalent to 0.6%, but at low pressure readings the error may be 5% or more.

IV EXPERIMENTAL PROGRAM

A. Scope of Experiments

Fluid friction due to both steady and unsteady flow in a 1" diameter conduit was determined for turbulent flow in the region of a fully developed boundary layer. Steady flow runs were made with Reynolds numbers from 75,000 to 750,000 (average velocities about 9 to 85 ft/sec). Unsteady flow runs were made with average velocities from about 15 to 72 ft/sec and average accelerations from zero to about 35 ft/sec^2.

As was explained on page 18 for the steady flow tests, differential pressures were averaged from the readings between taps at 60" and 79.5", and 79.5" and 99", and 60" and 99" from the entrance to the test section, and when the calibration shifted for any one gage (i.e. span) during a run, the readings from that gage were not included. On the other hand, for unsteady flow runs, only the differential pressures on the span from 79.5" to 99" from the entrance to the test section were used because this data was the most consistent.

It should be emphasized at this point, however, that the data from all three spans indicated the same trends in all portions of the unsteady flow runs. In runs where the calibrations of the gages on all three spans were constant, the average values could have been used, and the results would have been very close to those obtained from the one gage alone. A procedure of using only those unsteady funs where all gage calibrations remained constant, however, would have materially reduced the data available for calculation.

The practice of accelerating from one steady velocity to another during the unsteady flow runs (as described on page 19) produced similar patterns of average velocity and average acceleration for all runs. In order to obtain the best accuracy in scaling data from the records, however, amplification of the

signals from the differential pressure cells was regulated to give full-scale chart deflection for different portions, or phases of the runs. These phases have arbitrarily been called the initial impulse or transition from steady to accelerated flow, established acceleration, and the gradual transition from accelerated flow to steady flow.

1. Initial Impulse or Transition from Steady to Accelerated Flow:

This phase of the accelerated flow pattern is best shown in Figure 12. It includes the range from an established steady flow at t = 0 to the point where the acceleration has reached its maximum value. In Figures 12 a and 12 b, this is at 1.0 seconds and 1.1 seconds respectively. For these runs the ranges of the differential pressure cells measuring pressure drop along the test section was set for zero to 6 ft/ft, which represented the full maximum range of linear output from the amplifiers and power supplies. The test runs shown in Figures 13 and 14 also include this initial impulse phase, but the pressure cells were not set to include the head loss and velocity measurements associated with it. In Figure 12 a, the maximum acceleration was 36 ft/sec^2 and the maximum rate of change of acceleration was 77 ft/sec^2/sec. In Figure 12 b, these values are 30 ft/sec^2 and 100 ft/sec^2/sec respectively.

2. Established Acceleration Phase:

This phase represents the range following the peak acceleration where acceleration is decreasing or is nearly constant. Figures 12, 13, and 14 all show this phase to some degree, but for the runs shown in Figure 13, the ranges of the pressure cells were set for zero to 12 ft/ft to cover it more completely than for the others. The rate of decrease in acceleration for this portion of the runs in Figure 13 a to 13 f is from -2.0 ft/sec^2/sec to -14.4 ft/sec^2/sec. Acceleration rates were from zero to 30 ft/sec^2.

3. Gradual Transition from Accelerated to Steady Flow:

This phase is illustrated in the runs shown in Figures 14 a and 14 b. The primary value of these runs is to demonstrate that the measured pressure drop in the unsteady flow tests becomes the steady flow value when the transition occurs and to thereby serve as a check on the accuracy of measurements.

B. Presentation of Results

Results of the experimental work are encompassed in Figures 11, 12, 13, and 14. Figure 11 shows the experimental points determined from steady flow operation of the tunnel plotted on the familiar smooth pipe friction factor curve and summarizes the steady flow experiments. Results of unsteady flow runs are given in Figures 12, 13, and 14. In these figures for unsteady flow, curves are drawn for the instantaneous values of average velocity ($\bar{u}$) or (Q/A), average acceleration ($\bar{a}$) over the cross section, measured head drop, and the equivalent steady flow head drop. The latter is calculated using the instantaneous velocities in the steady flow head loss equation. The sum of the equivalent steady flow head loss and the acceleration head are shown by the small crosses at 0.1 second intervals, and the curve of measured instantaneous head drop is broken to accommodate these crosses where the values nearly coincide.

C. Analysis of Results

1. Steady Flow Runs:

In developing the tunnel and instrumentation, the aim was to evolve an apparatus which could readily produce unsteady flow patterns, and instruments with high frequency response to "instantaneously" record the variables. They should not be expected to compete with systems employing constant head tanks and micro-manometers for determining steady flow friction factors. Figure 11 shows, however, that the steady flow friction factors form a good cluster about the logarithmic smooth pipe friction curve. In this figure, the maximum deviation is 3.5%, but most points fall within 1% to 1-1/2% of the values on the curve.

2. Unsteady Flow Runs:

In Figures 12, 13, and 14, the small crosses at 0.1 second intervals provide a ready means of comparing the measured pressure drop along the tube with the values obtained by combining the acceleration head and the steady flow head loss based on the instantaneous average velocity. For comparing wall shear stress (τ_o) values, it is more convenient to subtract the acceleration head from the measured head drop curve and to compare the difference with the steady state friction head loss curve. In the discussions which follow, the variation of τ_o for unsteady flow from that for steady flow was calculated in this manner.

As was noted on page 21, these runs have been divided arbitrarily into three phases: (1) initial impulse, (2) established acceleration, and (3) gradual transition from accelerated to steady flow.

(a) Flow with Established Acceleration: The maximum variations of the unsteady flow τ_o from the steady flow value for the runs shown in Figures 12, 13, and 14 are as follows:

Fig.	Run	Ave. Velocity $\bar{u}$	Ave. Accel. $\bar{a}$	Maximum variation of τ_o: $\frac{(\tau_o)_{\text{unsteady}} - (\tau_o)_{\text{steady}}}{(\tau_o)_{\text{steady}}} \times 100$
12a(end)	40-2	42	35	+ 1.30%
b(pts)	40-10	39	30	+ 1.85
13a	38-4	55	16	+ .47
b	38-6c	57	10	+ .74
c	39-2	57	17	+ .21
d	39-4	53	17	+ .87
e	39-16c	59	13	- .48
f	39-20A	50	18	- .77
14a	38-6A	45	19	- 1.53
b	39-20B	43	23	+ 1.75

This tabulation shows a random variation of the τ_o values for unsteady flow from those for steady flow which is within the variation of experimentally determined steady flow friction factors from the average (smooth pipe friction

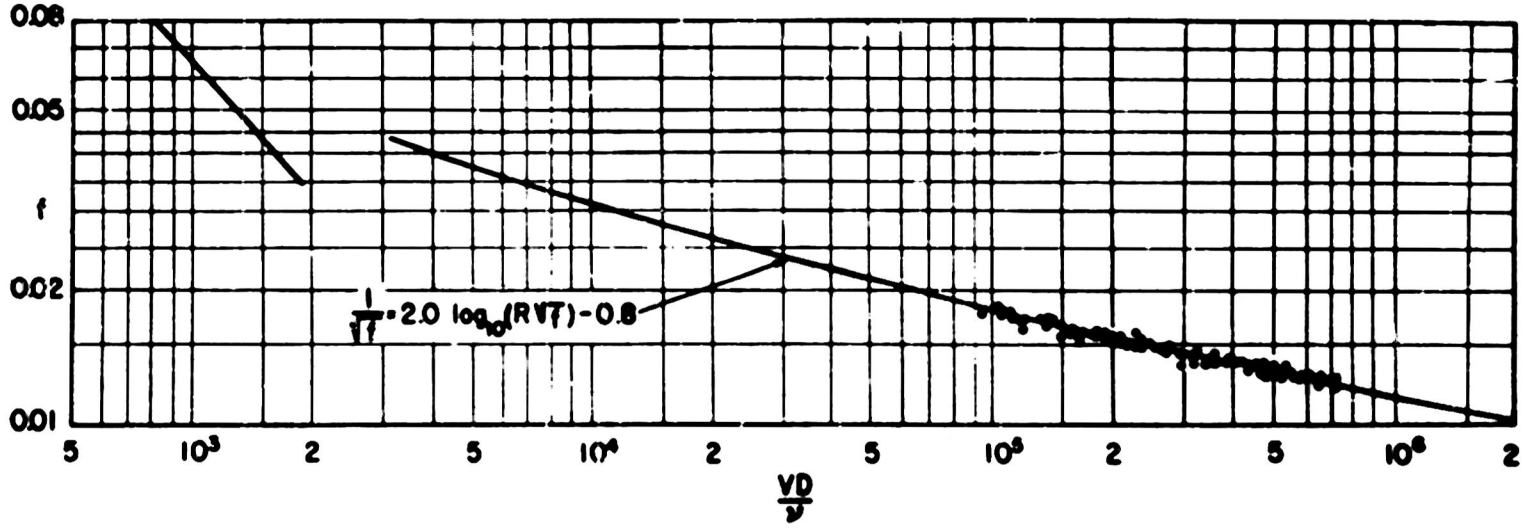

Fig. 11: Experimental Steady Flow Friction Factors Plotted on Smooth Pipe Curve

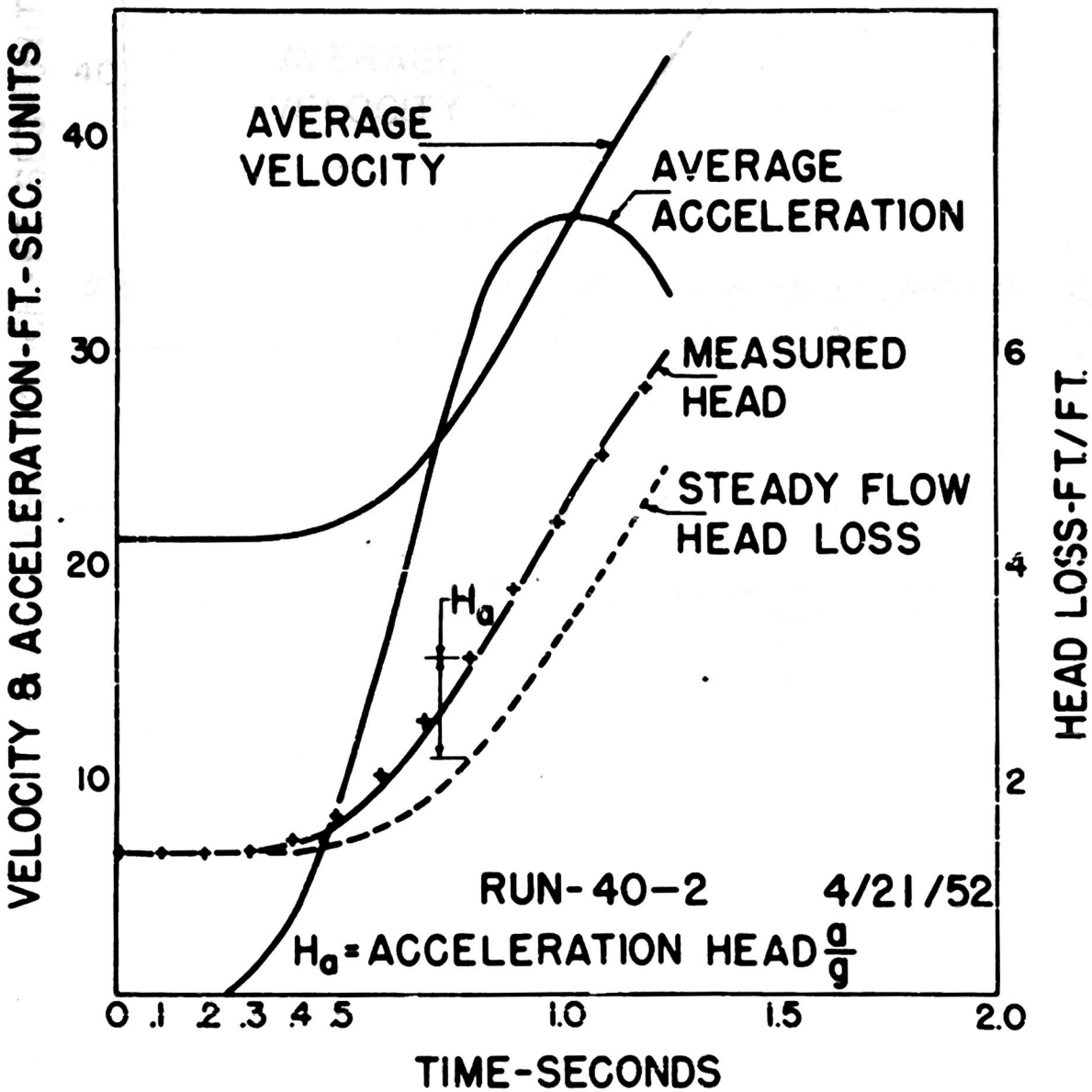

Fig. 12a: Unsteady Flow Run - Initial Impulse from Steady to Accelerated Flow

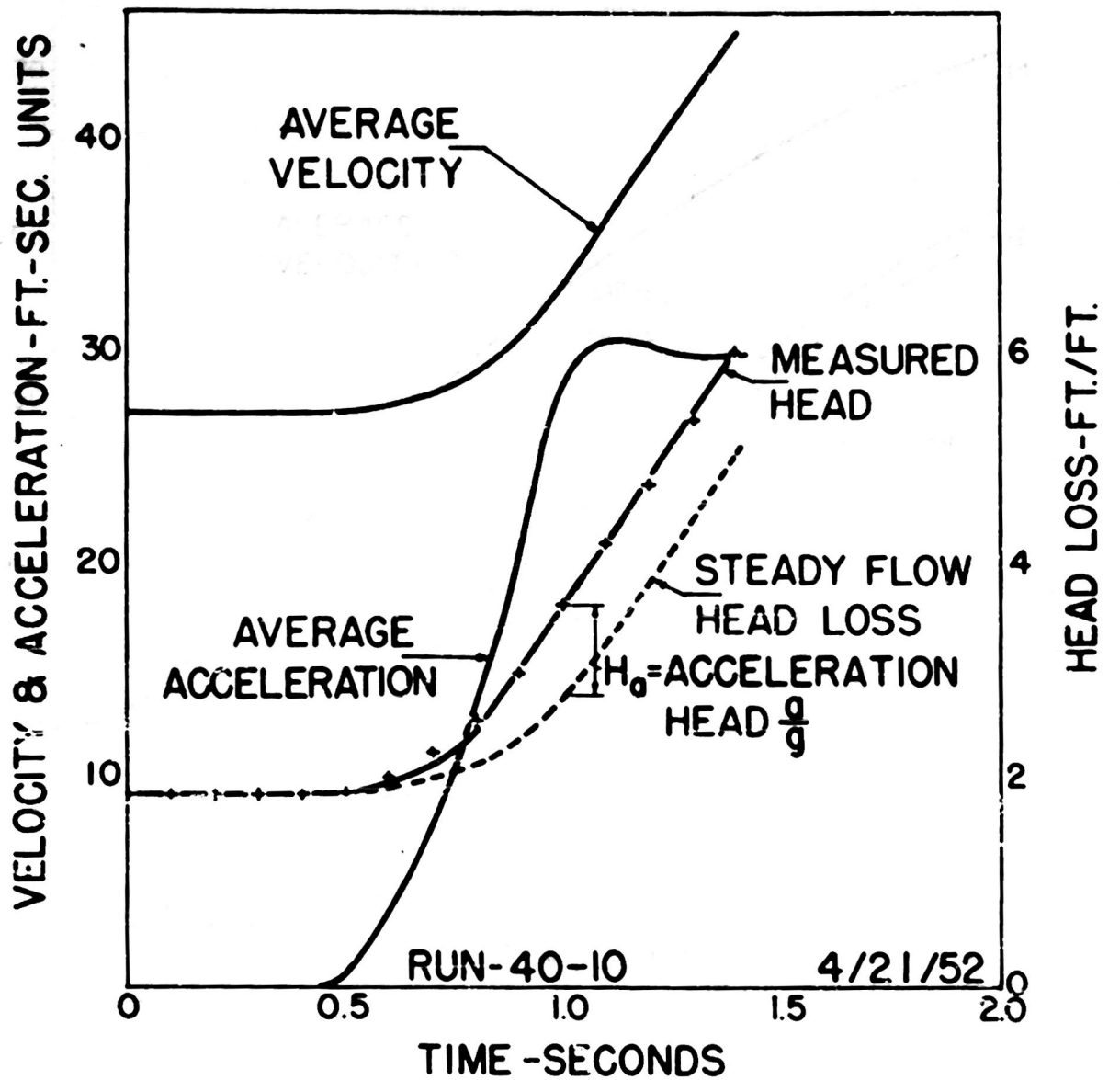

Fig. 12b: Unsteady Flow Run - Initial Impulse from Steady to Accelerated Flow

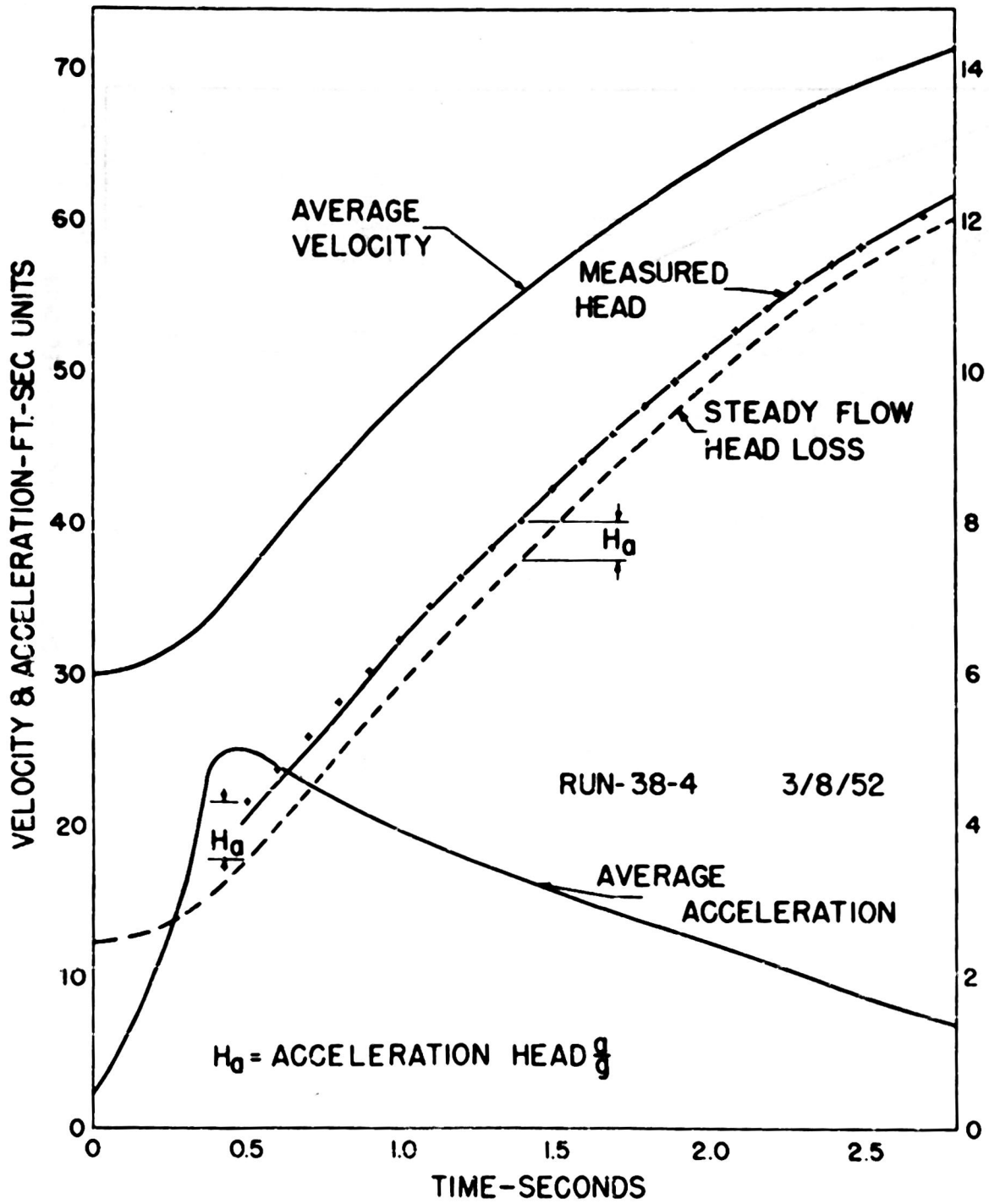

Fig. 13a: Unsteady Flow Run - Established Acceleration Phase

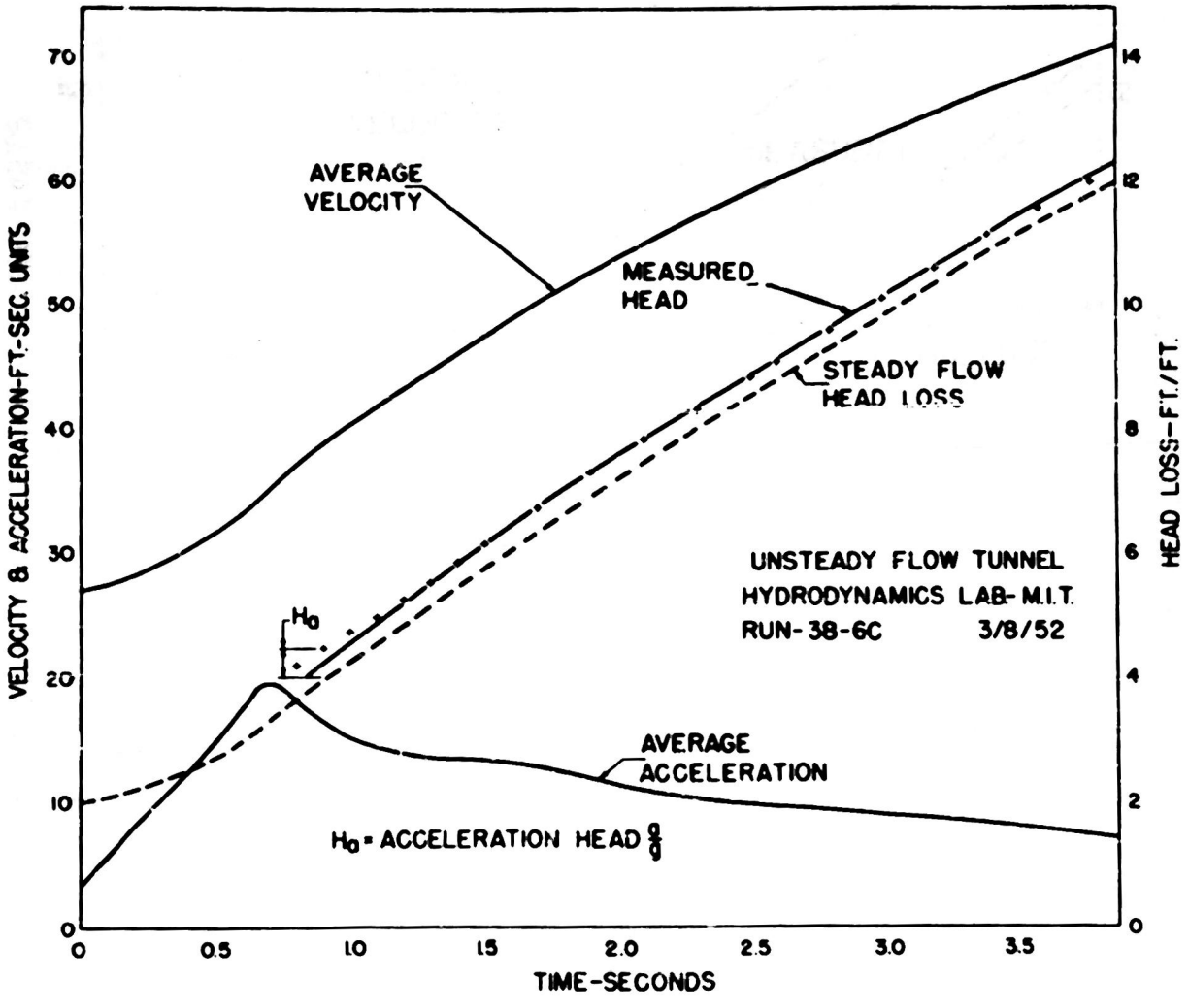

Fig. 13b: Unsteady Flow Run - Established Acceleration Phase

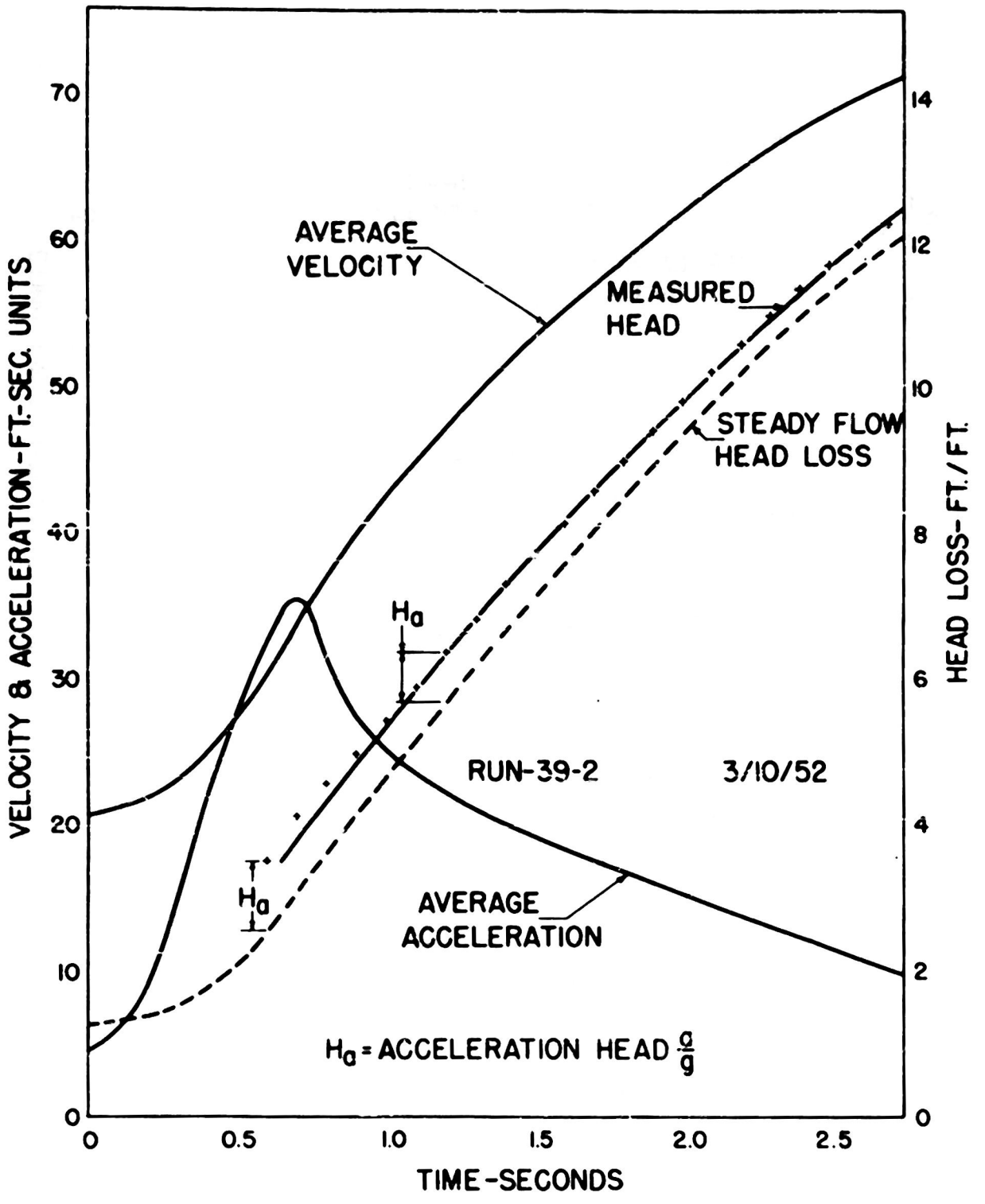

Fig. 13c: Unsteady Flow Run - Established Acceleration Phase

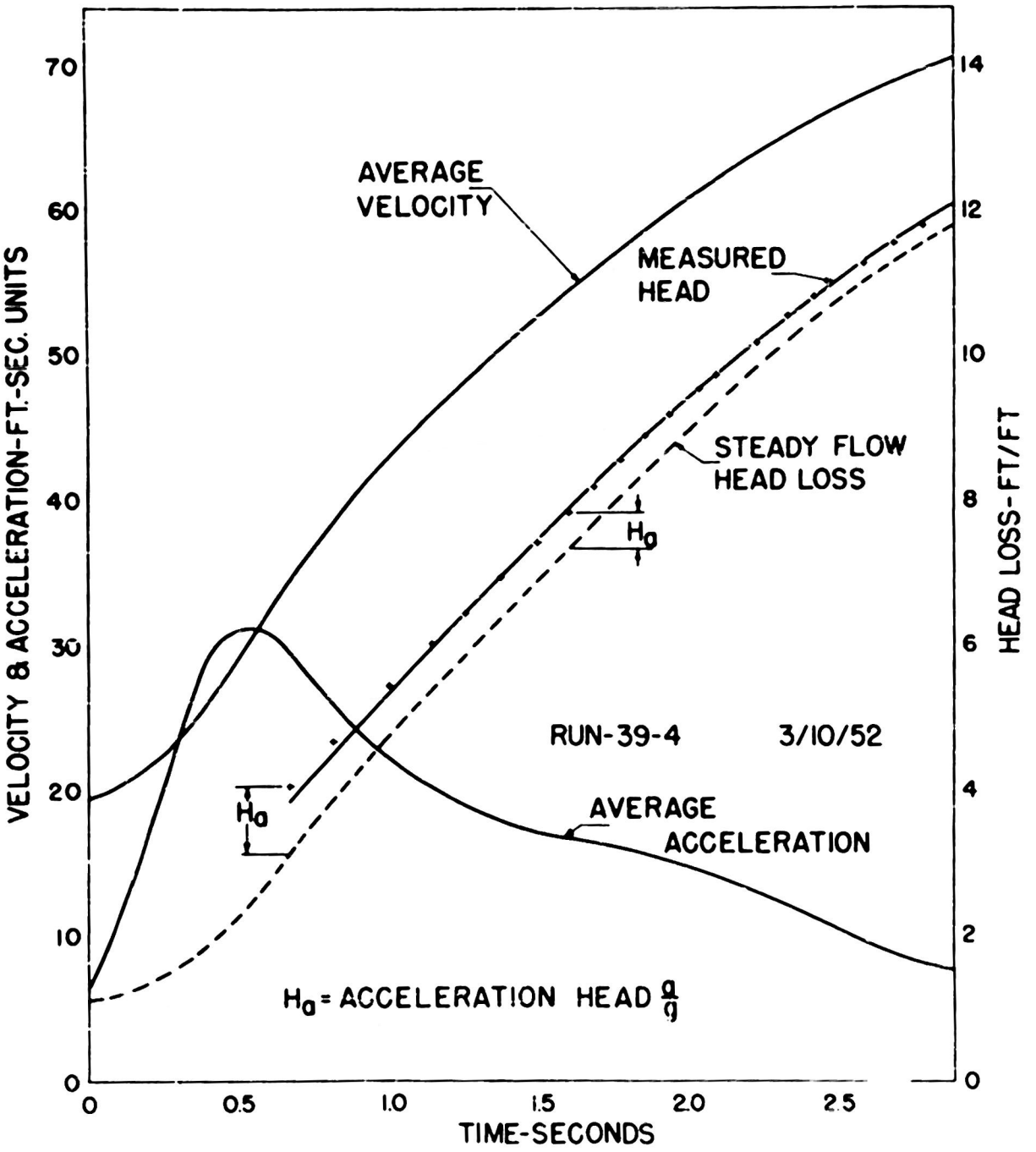

Fig. 13d: Unsteady Flow Run - Established Acceleration Phase

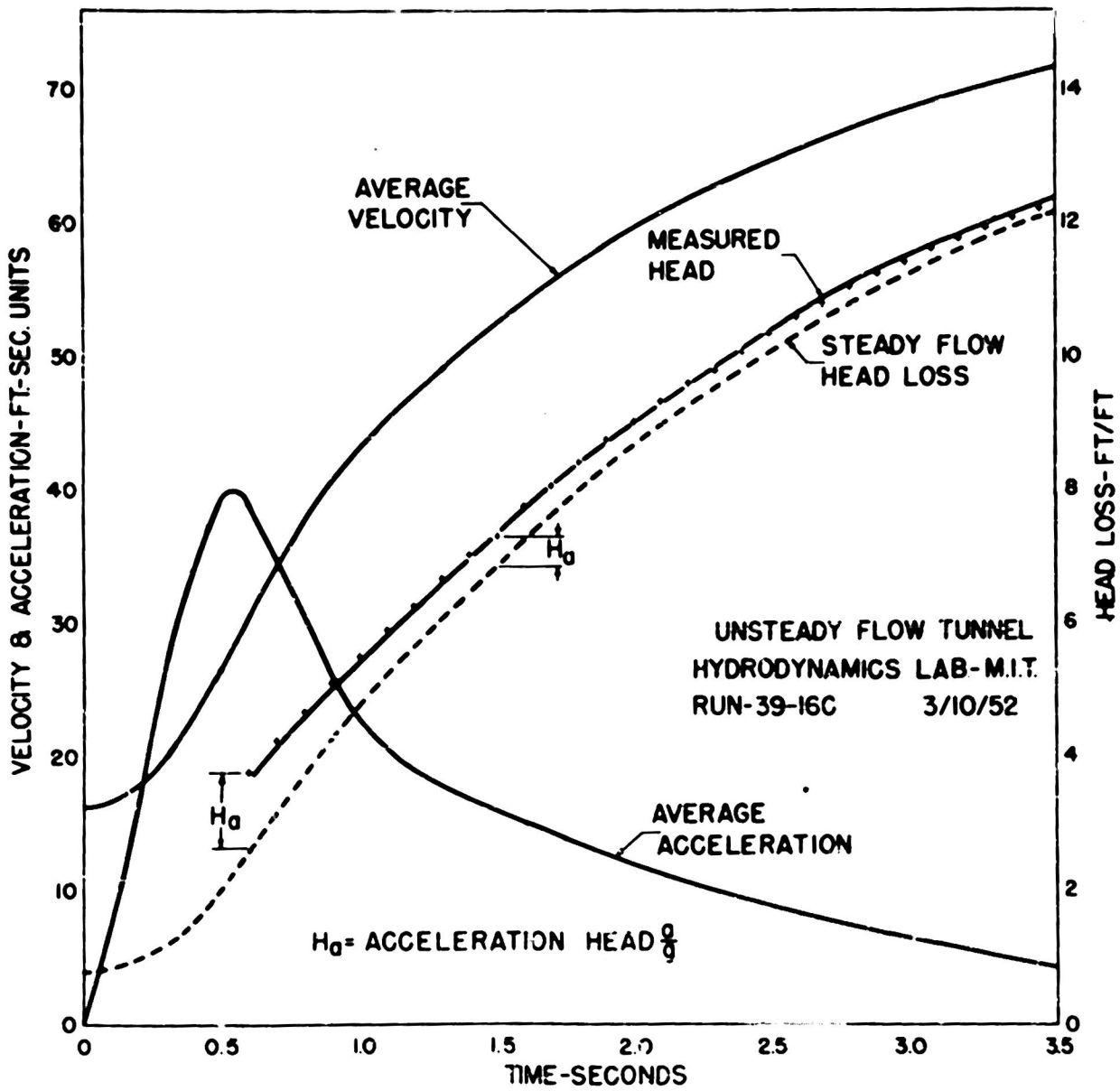

Fig. 13e: Unsteady Flow Run - Established Acceleration Phase

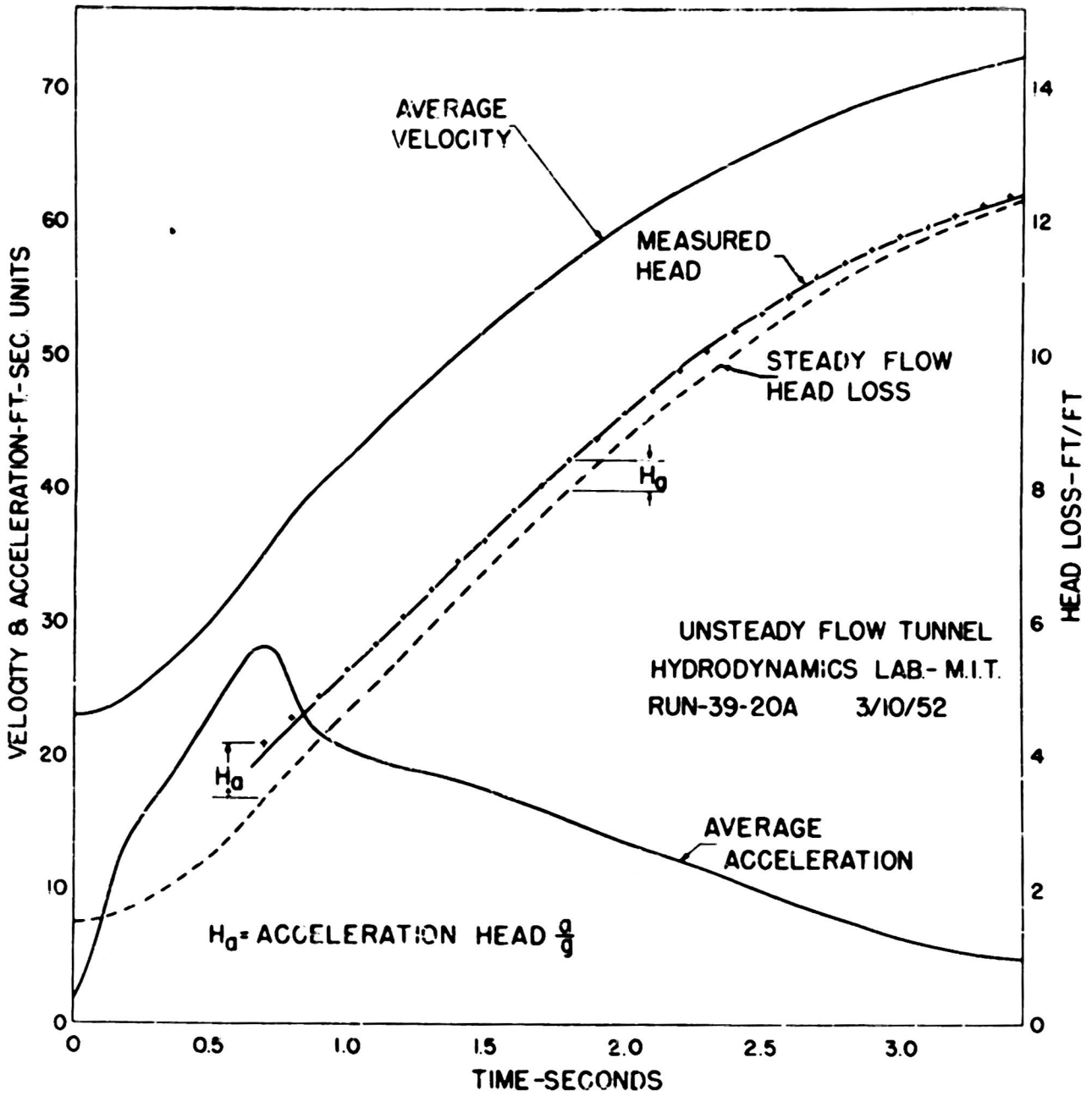

Fig. 13f: Unsteady Flow Run - Established Acceleration Phase

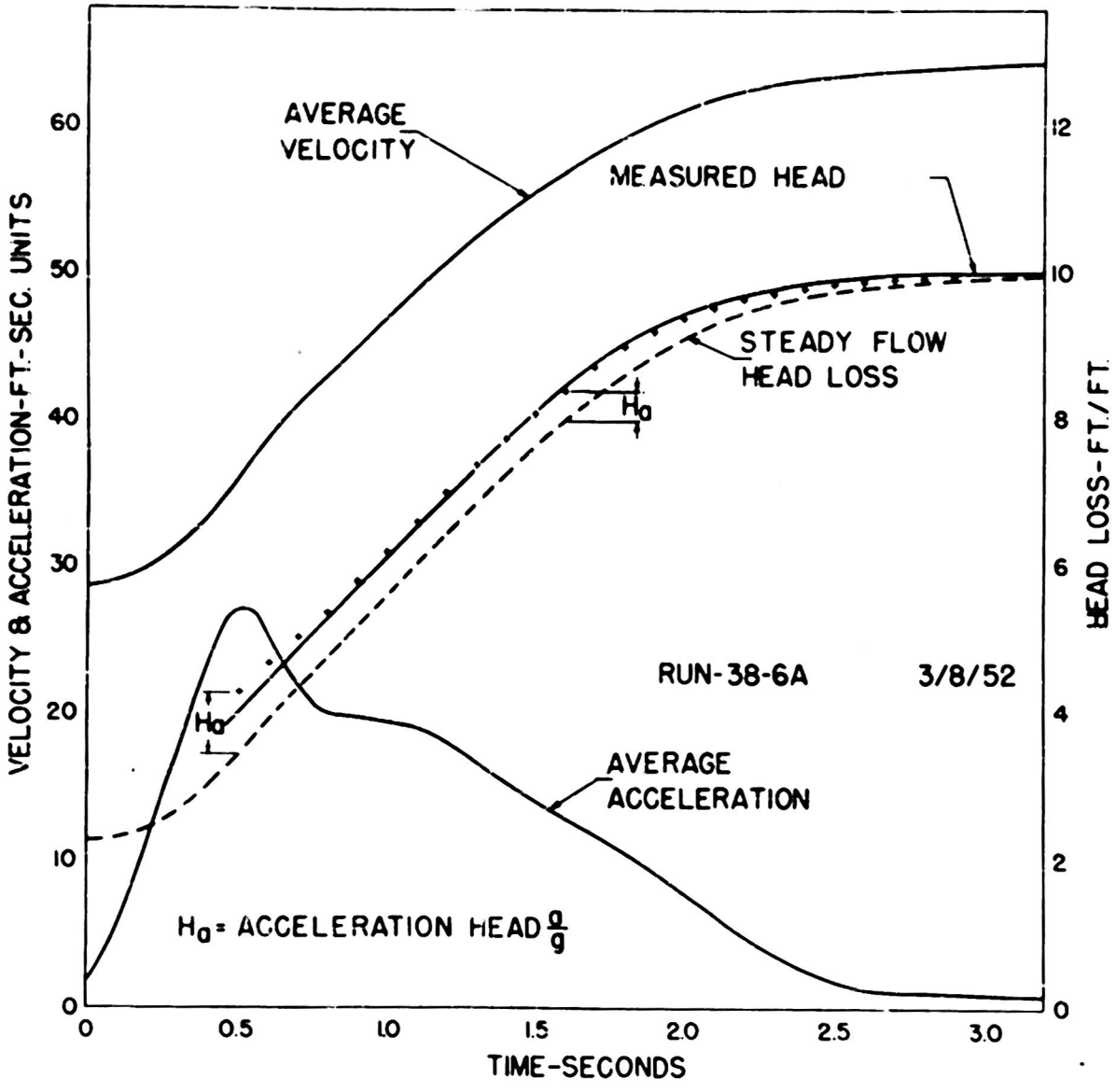

Fig. 14a: Unsteady Flow Run - Transition from Accelerated to Steady Flow

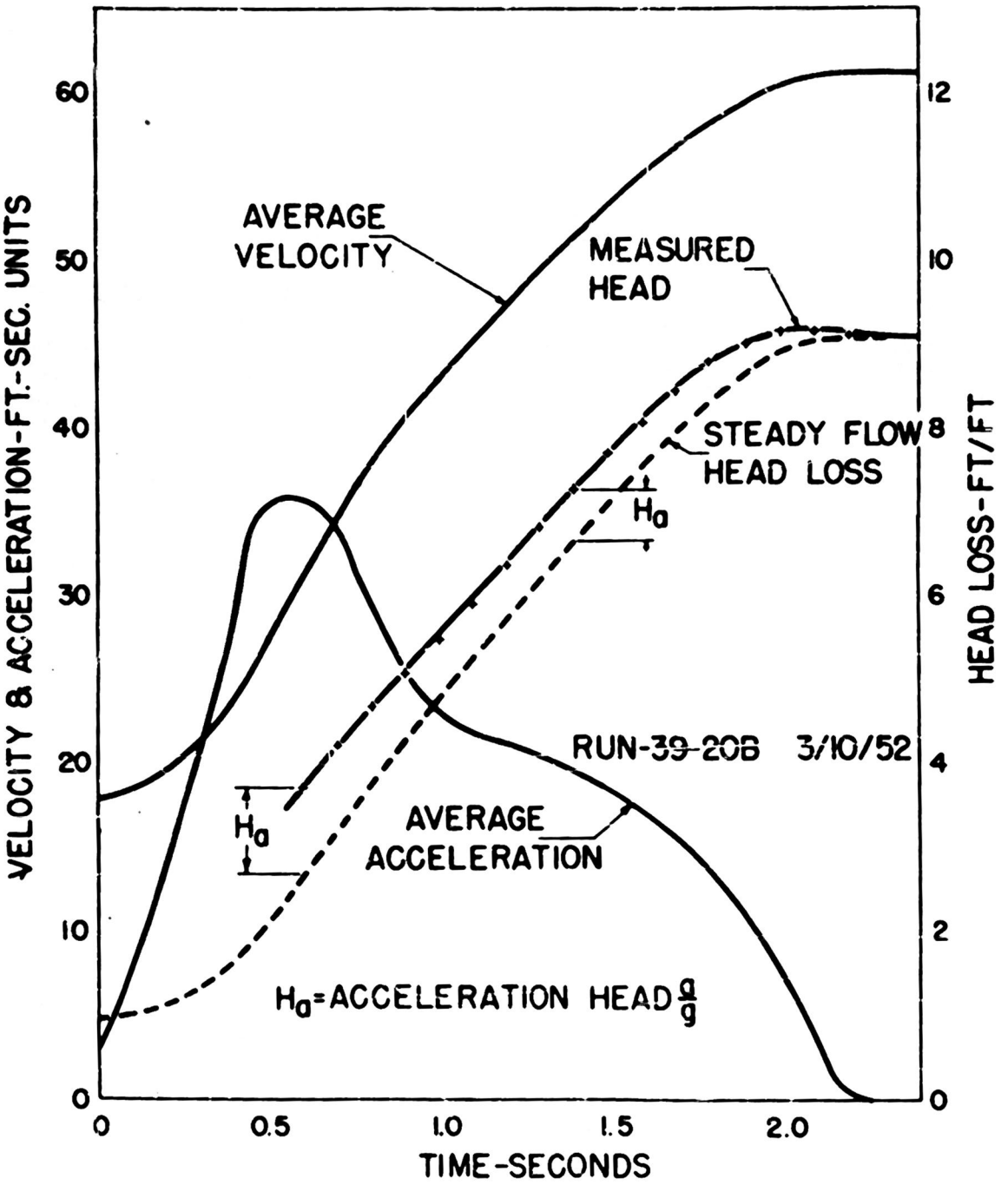

Fig. 14b: Unsteady Flow Run - Transition from Accelerated to Steady Flow

curve) in Figure 11. In other words, the experimental work indicates that when the acceleration is established and is not changing rapidly with time, there is no appreciable difference between the values of τ_o for unsteady flow and steady flow. As was noted on page 21, the experiments included accelerations of from zero to 30 ft/sec^2 and rates of change of acceleration from - 2 ft/sec^2/sec to -14.4 ft/sec^2/sec. As discussed on page 7, this indicates that the form of the acceleration distribution profile must be very similar to the velocity distribution profile.

(b) Initial Impulse Phase: The test runs shown in Figures 13 and 14 indicated that there was a consistent difference in the unsteady flow τ_o from the steady flow value during the initial impulse. It did not appear to be fair to judge wholly from these runs, however, because this difference occurred at the lower portion of the range settings of the differential pressure cells. As discussed in Section III E on page 20, this is the region of maximum error in converting data from the charts. To further investigate this region additional tests were performed in which the ranges of the differential pressure cells were set so that the differential pressures at the initial impulse were approximately at the middle of the ranges. Figures 12 a and 12 b show the difference between the measured unsteady τ_o and the steady τ_o to be as follows:

Fig.	Run	Time (sec)	Ave. Velocity $\bar{u}$	Ave. Accel. $\bar{a}$	Maximum variation of τ_o: $\frac{(\tau_o)_{\text{unsteady}} - (\tau_o)_{\text{steady}}}{(\tau_o)_{\text{steady}}} \times 100$
12 a	40-2	.40	21.5	3.5	- 3.0%
		.50	22.0	8.5	- 5.7
		.60	23.0	16.0	- 8.5
		.65	24.0	20.0	- 9.0
		.70	25.0	24.0	- 7.1
		.90	31.0	35.0	- 2.2
12 b	40-10	.60	27.5	3.5	- 3.6
		.70	28.0	8.0	- 6.4
		.80	29.0	13.0	- 5.1
		.90	30.5	20.7	+ 1.3

the maximum deviation occurs during the period of maximum rate of change of acceleration rather than at the maximum acceleration. In both cases, at the maximum acceleration the measured head drop agrees well with the value computed from the sum of the acceleration head and the steady state head loss. In Figure 12 a the maximum rate of change of acceleration is 77 ft/sec^2/sec, and in 12 b it is 100 ft/sec^2/sec.

In turbulent flow in a conduit, the shear stresses within the central core are primarily due to turbulent velocity fluctuations. As discussed on page 7, it is indicated that a finite time may be required for the velocity fluctuations to rearrange themselves. At the instant the accelerating force is applied, the motion of all filaments is resisted by shear stresses which are the same as those of steady flow. As the velocity increases due to the

accelerating force, the filaments near the wall are resisted by increased viscous shear. The shear on the filaments within the central core, however, cannot change until the velocity fluctuations change. If the latter require a finite time to change, the central portion of the flow will be accelerated more than that at the boundaries. The net effect is to produce a velocity gradient at the wall during a rapid impulse which is less than would be expected for the instantaneous average velocity of flow through the tube. In this sense, the instantaneous velocity profile form can be said to become "more peaked," and correspond to the third possibility (d) discussed on page 7. As discussed on pages 7 and 8, the exponential forms of velocity distribution can be used to illustrate this phenomenon. In Figures 12 a and 12 b, the value of τ_o for unsteady flow during a sudden impulse was found to be up to 7% less than that for steady flow at the same instantaneous velocities. This deviation occurred at velocities of 25 to 30 ft/sec, and Figures 3 and 4 on page 6 indicate that this change would be approximately equivalent to a change from m = 1/8 to m = 1/6 in the exponential velocity distribution law.

If the observation that these deviations occur only during high rates of acceleration is typical, it would indicate a possible lag in the setting up of the eddy generating mechanism. Once the generating mechanism has "overcome the shock," turbulence is generated at a rate sufficiently in balance with other conditions to give no appreciable differences from steady motion.

(c) Gradual Transition from Accelerated to Steady Flow: The transitions shown in Figures 14 a and 14 b are gradual, and the maximum variation of the unsteady flow τ_o from the steady flow value is 0.6%, which is of the same order of magnitude as experimental inaccuracy. As was pointed out on page 21, the primary purpose of these runs was to make certain the pressure cells indicated reliable pressure drops after the sharp rises in pressures to which they were subjected during the runs.

These tests were in no way counterparts of the initial impulse phase. Such a counterpart would entail high (negative) rates of change of acceleration for periods of time comparable to those in the initial impulse phase. It could also be produced by rapidly decelerating a steady velocity flow. (Note that this could be done on the present tunnel by arranging to rapidly introduce high-pressure air to the lower tank.)

It can only be concluded from these tests that they further verify the results of the established acceleration phase runs; namely, that there is no appreciable difference between the steady flow τ_o and the unsteady flow τ_o values for nearly constant rates of acceleration. On the other hand, if a steady flow were decelerated with a high rate of change of deceleration, it is probable that the shear stresses in the central core due to velocity fluctuations would not change immediately. In this case, however, the shear stresses on each filament aid the decelerating force, and the layers near the wall are probably retarded more rapidly than those farther from the wall. Such action would lead to higher velocity gradients at the wall and consequently higher values of τ_o than for steady flow at given instantaneous velocities.

It should be noted for these observations on the effect of rate of acceleration that the deviations from steady flow friction, although consistent, are small percentagewise. Furthermore, it is possible that these deviations could be explained by consistent measuring errors. Thus, while the instrumentation and the experimental measurement and data reduction techniques appear reliable, as was discussed in Section III and is considered further in the Appendix, these items are being scrutinized carefully in anticipation of additional confirming experiments. The above conclusions, consequently, are considered tentative.

V SUMMARY OF CONCLUSIONS

These experiments with fully developed turbulent flow in a conduit indicate the following variations from steady flow phenomena based on the arbitrarily selected phases of unsteady flow studied.

1. Established Acceleration Phase:

   (a) No appreciable change in τ_o value.

   (b) Approximately the same velocity distribution law.

2. Initial Impulse Phase:

The variations in the following properties appear to be a function of the rate of increase of the acceleration and not of the actual magnitude of acceleration. The variations from steady flow noted below are for periods of rapidly increasing rate of acceleration.

   (a) τ_o is less than for steady flow based on the instantaneous average velocity.

   (b) Velocity distribution is apparently "more peaked" than in steady flow.

   (c) Shear stress distribution is not linear. While shear is still maximum at the wall and zero at the center, at intermediate points it probably is less than is indicated by a linear distribution.

3. Rapid Increase in Rate of Deceleration:

This phase was not studied experimentally, but it appears reasonable to draw the following conclusions on variations from steady flow based on the results of the initial impulse phase and analytical consideration.

   (a) τ_o would be higher than for steady flow based on the instantaneous average velocity.

   (b) Velocity distribution would appear to have higher gradients at the wall than in steady flow.

   (c) Shear stress would be maximum at wall and zero at center but probably higher at intermediate points than in a linear distribution.

The observations concerning the rate of acceleration or deceleration are based on measured differences that are small percentagewise and are considered tentative pending additional confirming experiments.

APPENDIX

DIAPHRAGM DIFFERENTIAL TRANSFORMER TYPE DIFFERENTIAL PRESSURE CELLS

A. General

The diaphragm type differential pressure gage developed on this project incorporates a small differential transformer, which has light weight moving parts, does not require close clearances, and can be operated for at least several months under water. Its development is the outgrowth of studies and experiences reported in Reference (2).

The operating principle of the differential transformer sensing element can best be explained by referring to Figure 15.

The transformer consists of a small iron core and three coils wound side by side on the same axis. The center coil is the primary winding, and the other two are secondaries connected in phase opposition. When the core is centered, the same voltage is induced in each secondary and the net output is zero. The core is then said to be at its null point. Movement of the core in either direction causes an increase in the coupling between the primary and one secondary coil and a decrease between the primary and the other secondary coil, resulting in a net voltage output which is linearly proportional to the travel of the core.

The core is connected by a brass rod to a diaphragm as shown in Figures 16, 17, and 18, and movements of the diaphragm are thus detected and amplified. If the diaphragm deflection is linear with applied differential pressure, the output signal from the transformer is also linear with this differential pressure.

B. Construction Details

Figure 18 shows the assembled differential pressure cell in cross section. Details of mounting the diaphragm and field coils are shown in Figures 16 and 17. Pressure is admitted to both sides of the corrugated diaphragm through ports A and B. The gage is normally employed with the greater pressure at port B, and the following descriptions are for this arrangement; however, the cell performs satisfactorily with the greater pressure at port A. As the diaphragm deflects, the core moves longitudinally along the axis of the coils and a signal is generated as described in the preceding section.

All metal parts of the pressure cell are made of brass with the exception of the diaphragms, which are corrugated beryllium copper or Inconel. The case was made heavy to guard against distortion at pressures up to 200 psi where the gages are sometimes employed.

The corrugated diaphragms used as the sensing element were originally made for capsules for aeronautic instruments and controls, and they were received with a skirt around the periphery. This skirt was utilized in mounting in the following manner: A heavy brass ring was machined with a groove and a lip, as shown in Figure 17. The lip was machined to match the contour of the diaphragm at the edge and so that the skirt on the diaphragm had to be pressed lightly over

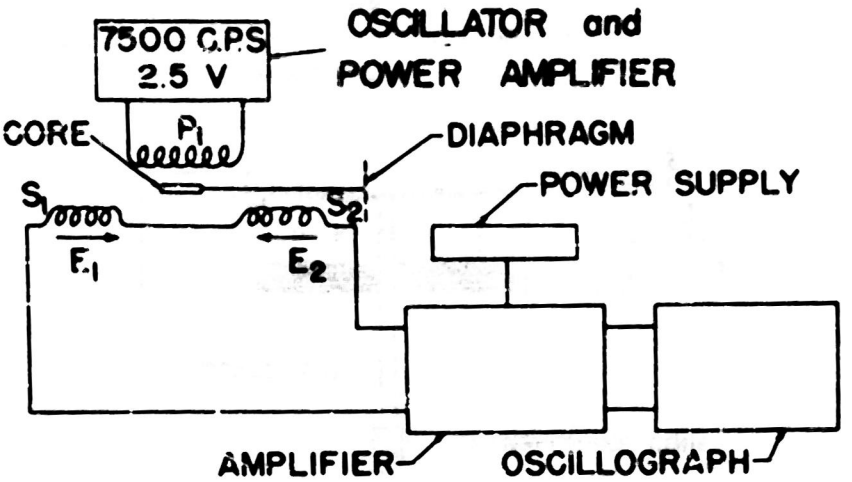

Fig. 15. Schematic Diagram of Electronic Principles Employed in Differential Pressure Cell

Fig. 16: Diaphragm, Cage, and Transformer Assembly

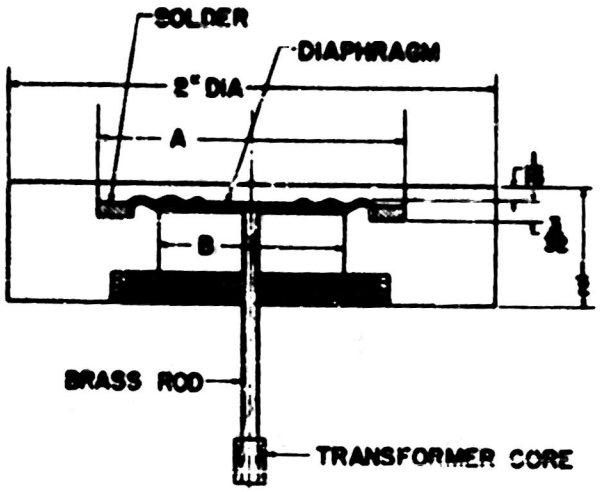

Fig. 17. Details of Mounting Diaphragm and Transformer Core

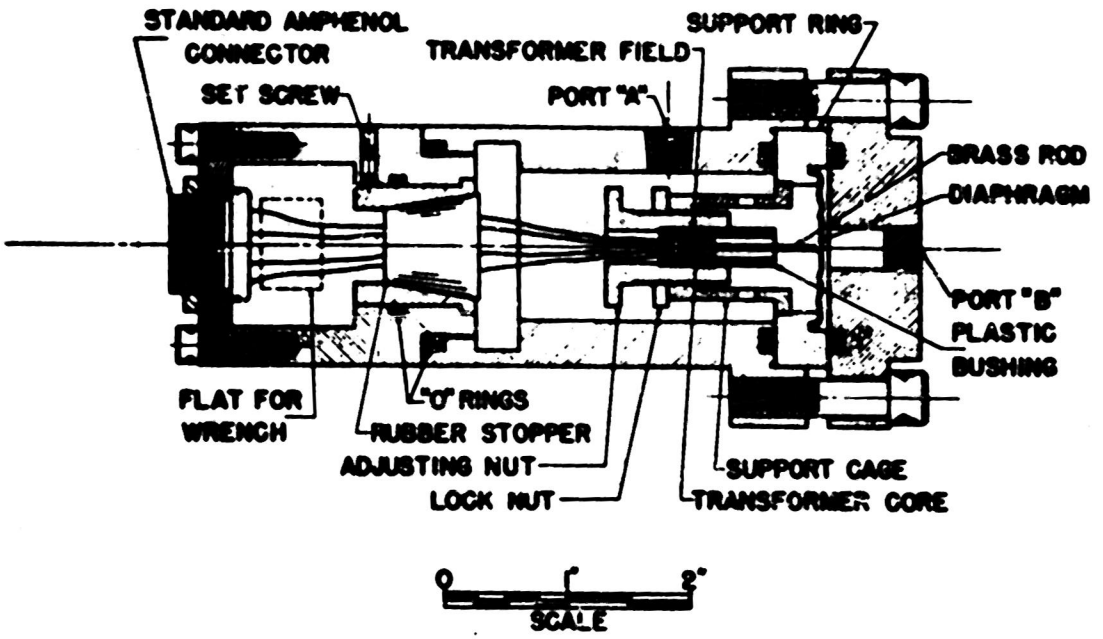

Fig. 18. Cross-Sectional View of Type DDT Differential Pressure Cell

he lip, causing a slight radial tension. The groove was then filled with pieces of solder, the diaphragm was held in place with a weight, and the assembly was rotated on a small rotary table while a small torch played on the edge of the ring to melt the solder. This job could also be done in a controlled electric oven. Soft solder was used in the groove for both the beryllium copper and the Inconel diaphragms. In early models, the Inconel diaphragms were silver soldered, but it was found that soft solder was just as effective as the silver solder and was much easier to apply.

The transformer coil housing is inserted in the adjusting nut as shown. The coil assembly fits loosely in the adjusting nut and is held in place by a lucite sleeve, which is a snug fit. This design permits the coil assembly to be removed without damage for inspection or recoating with waterproofing material.

Standard recommended practice is to support the coils in plastic and to keep all metal as far as possible from them. In early stages of development, hard rubber was used, but its low modulus of elasticity and high Poisson Ratio caused it to distort under pressure. Laboratory experiments disclosed that if the coil assembly is mounted in a brass cup, in such a way that the metal surrounding the coil assembly is approximately symmetrical, the characteristics of the transformer are as good as when the coil is surrounded by plastic. The location of the coils is not critical as long as the metal around them is approximately symmetrical; however, if the coil assembly is raised until it is flush with the top of the adjusting nut, the output almost vanishes. When the housing is half-way out of the nut, the output characteristics are fair, but the location becomes extremely critical, and change in location of a few hundredths of an inch causes the signal to vanish entirely.

The adjusting nut and coil assembly are coupled to the diaphragm support ring by a cage. This arrangement makes all relative motion between diaphragm and coils independent of the total hydrostatic pressure in the shell of the pressure cell. The adjusting nut screws in or out of the cage (40 threads per inch) to permit setting the transformer for the desired operating range as described in a later paragraph.

Lead wires from the transformer coils were coated with rubber cement and drawn through small holes drilled in a #1 rubber laboratory stopper and were soldered to an amphenol connector, as shown in Figure 18. The rubber stopper was coated with rubber cement and fitted into a brass bushing sealed with "O" rings and held in place by a set screw. When it is desired to change a transformer coil, the entire assembly of adjusting nut, coil, bushing, and amphenol connector are removed as a unit. All such units are interchangeable from gage to gage.

C. Sensing and Detecting Elements

1. Diaphragms:

Beryllium copper and Inconel diaphragms exhibit low hysteresis characteristics and appear to be the two best materials known for this service. Corrugated diaphragms are more linear and do not develop as much radial tension for a given deflection as flat diaphragms. Two types of diaphragms supplied by Ranco, Inc., of Columbus, Ohio, were used in these gages. The first is a 15/16" diameter by 0.0075"

thick Inconel diaphragm with three corrugations, and the second is a 1-7/32" by 0.0043" beryllium copper diaphragm with three corrugations. Each of these diaphragms was made to serve two pressure ranges. One pressure range was obtained by using their full diameter as shown in Figure 17. The second pressure range from each was obtained by reducing the diameter, B, to the next corrugation and soldering the diaphragm to the ring at this diameter. The reduced sizes are designated "half-size Inconel," and half-size beryllium copper" diaphragms.

2. Differential Transformer Elements:

These elements were supplied by Schaevitz Engineering Corporation, of Camden, New Jersey. Three sizes are used, 0.005L, 0.010L, and 0.020L. The number indicates the inches of travel of the core for which the output is linear, i.e. 0.005" etc. When the travel is greater than the rated value, the output is no longer linear. The coil assemblies are approximately 5/16" diameter by 3/8" long with a 1/8" diameter hole for the core, and the core is approximately 1/16" diameter by 5/32" long with a 0.030" hole for mounting. The Schaevitz Engineering Company cooperated with this project in developing suitable waterproofing techniques and now supply these transformers with a heat-treated coating of Glyptal Varnish on request.

D. Electrical Components

The electrical components associated with Type D D T Differential Pressure Cells consist of the following elements:

1. Oscillator:

A Hewlett Packard Model 200 C is used to excite the primary coils of the differential transformers. The output signal frequency is set at 7500 cps, this value being determined by experiments with the transformer to afford good stability and sensitivity.

2. Power Amplifier:

It was found necessary to supplement the oscillator with a power amplifier due to the low impedance of 6 differential gages in parallel. The input to the power amplifier was adjusted so that 2.5 volts were present at its output terminals when fully loaded. See Figure 19 for circuit details.

3. Amplifiers:

A separate amplifier serves each pressure cell. The electrical signal taken from the output terminals of the linear differential transformer is amplified and detected by means of the circuit indicated in Figure 19. V_1 and V_2 represent straight amplification of the input signal. The cathode resistor of V_1 was left unbypassed to introduce a small amount of negative feedback for stability purposes. C_6 was found necessary to reduce a small amount of parasitic osillation that occurred from feedback from associated channels wired on the same chassis. V_3 acts as a modified infinite impedance detector; C_7 is the detection capacitor acting in conjunction with R_{12} and R_{13}. The left half of V_3 is biased to cutoff by

proper selection of the grid to ground voltage of the right half of this tube. V_4 is a difference amplifier providing a high current source for the low impedence of the oscillograph. S_1 and J_1 permit the introduction of a calibration signal to the oscillograph, which is normally inserted between the cathodes of V_4 by means of the jack J_2. R_{20} permits the selection of the d.c. level of the output signal, while R_{17} permits a fine control of the output d.c. signal amplitude. The amplifier is designed for a 7500 cps carrier signal and the output to a 5 Ω load is linear between -8 to +8 ma. Two such amplifiers were constructed on a single chassis.

4. Power Supplies:

Two 300 volt, 70 ma electronically regulated power supplies were used in conjunction with the above mentioned amplifiers. During the experimental work described in this report, one power supply energized 4 amplifiers, while the other supplied power for the remaining two. The Power Supply circuit is indicated by Figure 19.

5. Recording Oscillograph:

The Hathaway Type S-8B recording oscillograph is used to photograph the output traces. A light beam is focused on a mirror set on the movable suspension of a galvanometer (No. OA-2) having a natural frequency of 750 cps. The input signal sets the galvanometer suspension in motion, causing the reflected light beam to vary accordingly over the surface of a moving photosensitized paper. The time scale of the record is obtained by a tuning fork arrangement that operates an independent shutter and light source system. This produces a set of equally spaced lines on the photographic paper. The overall system works in the following manner:

The oscillator and power amplifier energize the differential transformer with a carrier frequency of 7500 cps. The differential output of the secondary of this transformer varies according to its core position, which is determined by the instantaneous pressure in the system to be measured. This amplitude modulated signal is then amplified and detected. The detected voltage is placed upon the terminals of the oscillograph galvanometers, which in turn determine the trace of a light beam on the photo sensitized paper. The paper is developed with ordinary darkroom techniques and sample records are shown in Figure 8.

E. Performance

Desirable characteristics of a pressure cell are reliability of indication, ruggedness, and durability.

1. Reliability of Indication:

In general, reliability of indication means that once a gage is calibrated, a given indication or signal represents the same pressure which gave that indication during calibration. Factors tending to reduce reliability of an electronic diaphragm gage are:

a. Hysteresis
b. Shift of zero position

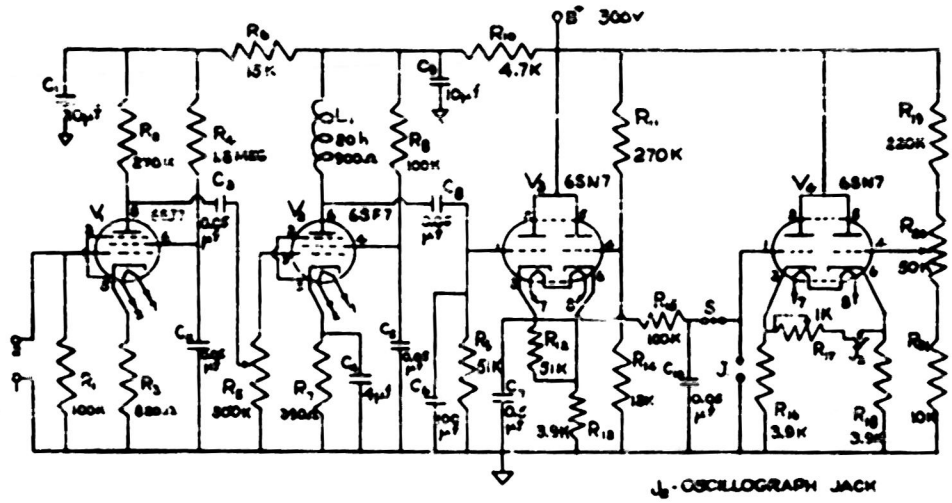

Amplifier for Pressure Cells

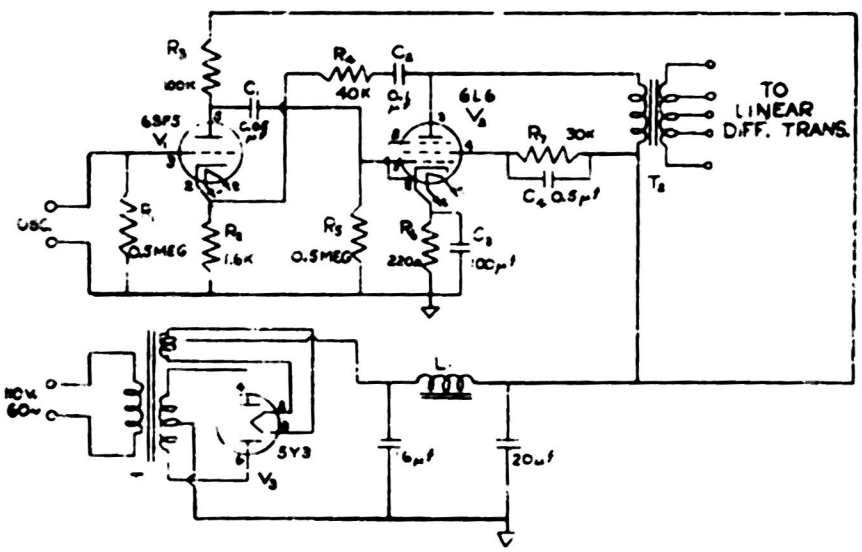

Oscillator Power Amplifier

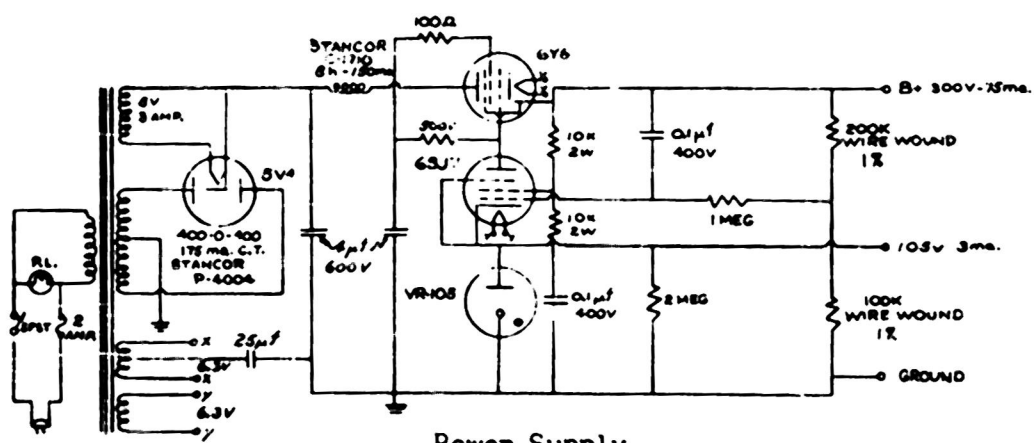

Power Supply

Fig. 19: Circuit Diagrams of Electrical Components for Differential Pressure Cells

c. Change in spring constant of diaphragm
d. Low frequency response (inability of diaphragm and sensing element to follow varying pressures)
e. Instability of the electronic element under conditions of normal use.

Hysteresis: If one carefully plots the output curve of a diaphragm pressure cell as he gradually increases the pressure and again as he gradually decreases the pressure, he usually finds two curves which may close at both ends but do not touch in the central region. This phenomenon is known as hysteresis and is due to failure of the diaphragm to recover immediately. If sufficient time is allowed between readings for the diaphragm to recover completely, this effect may go undetected. Hysteresis can be reduced by prudent choice of diaphragm material and proper mounting. The corrugated beryllium copper and Inconel diaphragms used in the gages under discussion showed hysteresis to be less than 1% of maximum applied pressure.

Shift in Zero Position: This effect is usually due to insufficient clamping at the edges or to overstressing the diaphragm. In the case of flat diaphragms, a considerable amount of radial tension is induced when the diaphragm is deflected. It has often been found, especially for stiff diaphragms, that the diaphragm slips away from its clamping at the edges under loading and then fails to slip back when the load is removed. In order to avoid this problem, diaphragms have sometimes been machined out of a heavy piece of metal, leaving a substantial ring at the edges for mounting. One successful method developed on this project for another gage (see Reference 2) consists of sweating a beveled ring to the diaphragm and clamping with a conical mating ring to give radial tension. In the differential pressure cells described herein, corrugated diaphragms soldered to a heavy ring with initial radial tension show no zero shift.

Change in Spring Constant of Diaphragm: This effect is usually due to temperature changes and for all practical purposes is negligible. When used in warm or cold fluids, the gages should be calibrated at the same temperatures.

Frequency Response: If a simple spring mass system is excited by a periodic force of the same frequency as its natural frequency, the force is said to be in resonance with the system, and the latter will vibrate with a larger amplitude than the exciting force. If the exciting frequency is very high compared to the natural frequency, the system will vibrate at its natural frequency. If, however, the exciting frequency is very low compared to the natural frequency, the system will vibrate at the frequency of the exciting force. In obtaining dynamic pressure measurements where the diaphragm is the spring and the mass includes that of the diaphragm and core (see Figure 17) as well as the water in the lead lines, only the third case can possibly give true indications of pressure pulses. It is customary to assume a gage suitable for measuring pulses of a frequency up to approximately 1/3 the natural frequency of the diaphragm sensing element.

Common practice is to rate pressure cells in air without accounting for the mass of fluid to be moved in lead lines, which is a variable of application. The natural frequencies of the four types of diaphragms used in this work were determined by exciting each with a 15 watt speaker driven by an oscillator and audio amplifier. The normal output was noted on an oscilloscope screen as shown in

Figures 20, 21. When resonant frequency was applied, the diaphragm vibrated with large amplitude and the signal appeared as in Figure 20 b. The results are tabulated below

Diaphragm Assembly	Natural Frequency in Air	Entire System
Full Size Be-cu	400 cps	- - -
Half Size Be-cu	1100 cps	165^{+} cps
Full Size Inconel	3000 cps	220^{+} cps
Half Size Inconel	6200 cps	300^{+} cps

Of greater interest in the study at hand than the natural frequency of the gage in air is the natural frequency of the gage as installed in the system. To approximately obtain this frequency, the gages were set in the running position and deliberately subjected to water hammer shocks by opening and closing the foot valve (see Section III-C). These shocks caused the diaphragms and water in the lead lines to vibrate and results were recorded on the oscillograph as shown in Figure 21. The large oscillations are due to the natural frequency of the water-air system, and the small oscillations are due to water hammer of the system with the diaphragm acting to effect a more elastic system. These frequencies represent those which the diaphragms can pick up and are below the actual natural frequencies. Inasmuch as the full size Be-cu diaphragms are used only for level measurements and are quite fragile, they were not subjected to the water hammer treatment. The recorded frequencies of the entire system for the other three diaphragms are shown in the right hand column in the above tabulation.

Instability of Electronic Elements: The transformer elements employed in these pressure cells appear to be very stable over periods of at least several months. It has been found, however, that it is difficult to obtain oscillators and amplifiers which are stable. For this reason, it is advisable to make frequent calibrations during test runs.

Ruggedness: The gages do not need to be handled with extreme care, and only when the most sensitive diaphragms are used with extremely high gain settings are the cells affected by normal room vibrations.

Durability: Once properly waterproofed, a cell gives long troublefree service under water. In some cases they have not been opened for adjustment for several months.

F. Application

1. Selection of Diaphragm-Transformer Combination:

Selection of the best diaphragm-transformer combinations for a given differential pressure measurement is largely a matter of experience. Of course, for pressures over 50 psi, only the "half size Inconel" diaphragm is strong enough to resist permanent set, while the beryllium copper diaphragms should not be used for pressures of more than about 12 ft. and 20 ft. of water for the full and half sizes respectively. However, even the full size Inconel diaphragms can be used with fair success in ranges of 0 to 10 ft. water for full 10" chart deflections, and the half size Inconel, good for about 100 psi, has been employed to give full 10"

(a) 6100 cps (b) 6200 cps

Half-Size Inconel Diaphragm

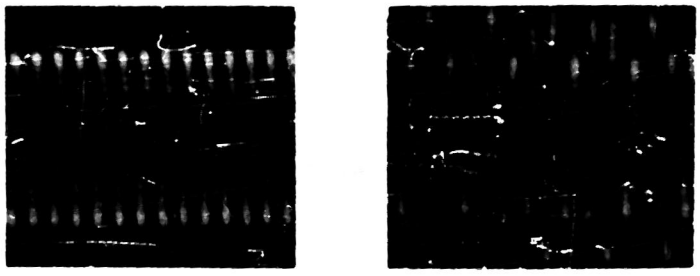

(a) 2900 cps (b) 3000 cps

Full-Size Inconel Diaphragm

Fig. 20: Photographs of Oscilloscope Screen During Diaphragm Natural Frequency Tests

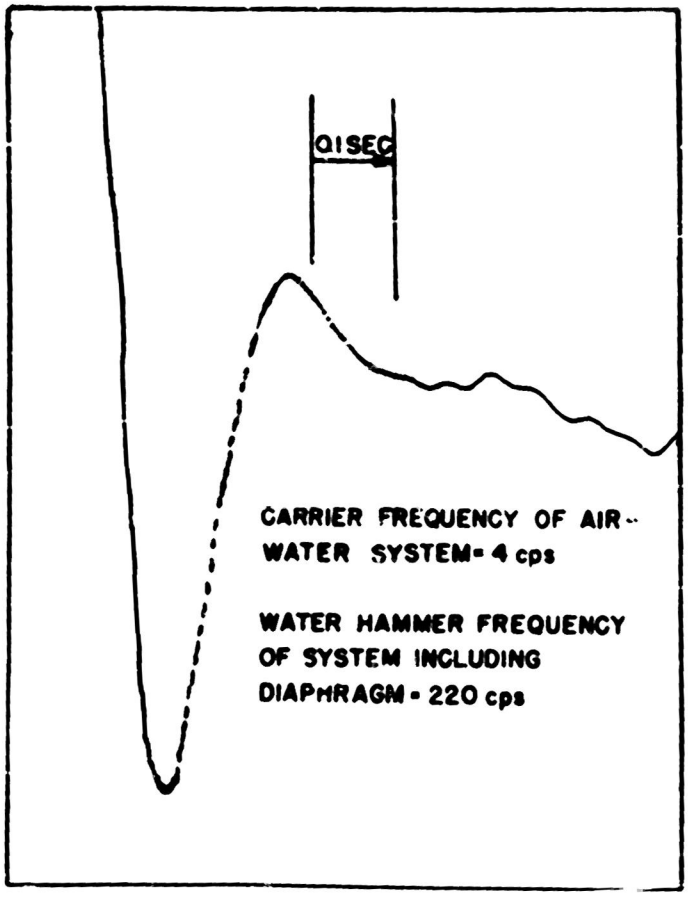

Fig. 21: Water Hammer Pulses of 220 cps Recorded with Full-Size Inconel Diaphragm

chart deflections for ranges as low as 0 to 15 psi. It is thus apparent that there is considerable overlapping in adaptability.

It has been observed that these corrugated diaphragms can be deflected to about 4% of their free diameters without incurring any residual set. For the smallest diaphragm, the half size Inconel, which is 0.5" diameter, this would mean a deflection of 0.020", or the full range of the largest transformers in use. Hence, it would not be possible to overload any diaphragm without noting the deviation from linearity of the output. From the standpoint of obtaining instantaneous measurements, the smallest total displacement is the most desirable, since this requires the smallest quantity of water to be set in motion in the lead lines. On the other hand, a very small movement of the diaphragm for full chart deflection requires the electrical amplification of the signal to be high; this often results in a shift in calibration due to only minute changes in the primary input voltage. Experience has shown that a diaphragm-transformer combination which under full pressure range allows the diaphragm to travel about 60% of the rated range of the transformer (i.e. 0.003" deflection of diaphragm for a 0.005; transformer), gives very satisfactory results. It should be noted that the full chart deflection can be obtained for ranges other than those starting from zero (viz., 3 psi to 9 psi rather than 0 to 6).

2. Setting Null Position:

Characteristics of the differential transformer used in the differential pressure cell are such that the output is linear with travel of the core within the range of the instrument. When the core is centered between the two secondary coils, it is at a null, or zero position. The net output of the transformer here is zero. The signal increases as the core moves away from this null point in either direction; however, in the vicinity of the null, the output changes only slightly with core movement. For this reason, the transformer is usually operated in a range which starts with the core a small distance from the null and allows it to proceed in the same direction from the null with increasing diaphragm deflection. Of course, comparable results can be obtained by starting some distance from the null point and allowing the core to approach the null position, so long as the "dead" region in the vicinity of the null is avoided. In the latter case, the signal would decrease with increasing deflections.

The procedure for setting the null position is best explained by referring to Figure 17. The cover is removed from the gage and the assembly of diaphragm, cage, and adjusting nut are removed from the gage body. The primary coil is excited (normally 7500 cps and about 2.5 volts), and the output signal is observed as a sine wave on an oscilloscope screen. By turning the adjusting nut in or out of the cage, the core is moved relative to the transformer coils. The null point is reached when the signal on the oscilloscope screen is a minimum. In practice, the nut is turned sufficiently to permit the core to advance slightly beyond the null point, so that when the diaphragm is loaded the motion will continue in the same direction.

When the desired setting is attained, the lock nut is tightened, the assembly pushed back into the gage body, and the cover replaced.

3. Procedure for Filling Gages with Water and Bleeding Piezometer Taps and Lead Lines:

No air pockets can be trapped in the gage or lead lines if the recorded pressure indications are to be "true". Air pockets compress with increased pressures and cause more flow to be set up in the lead lines than that required to depress the diaphragm. The inertia of the water thus set in motion induces errors both in the magnitude of the pressure changes and in the time at which the changes occur. Air pockets are reduced by bleeding the lead lines and piezometer taps and by evacuating the pressure cells before filling.

The procedures for evacuating the pressure gages are best explained by referring to Figure 9.

a. A Bourdon-type vacuum gage is attached at valve #4.

b. A short length of copper tubing is attached at valve #2.

c. A chemical laboratory type aspirator is attached to a faucet. Rubber tubing leads from the vacuum side of the aspirator to the above short length of copper tubing. This juncture is then immersed in a jar of water.

d. All valves on the gage "Christmas tree" are opened except #1.

e. When the vacuum reaches 28.5" o. .g. or more, the rubber tube is removed from the short copper tubing and water enters the cavity.

When the gage is filled, it is placed on the supporting rack and the pressure lead lines are attached. Each is then bled through the gage valves for several minutes before each set of runs. A piece of tubing attached to the bleed valve (No. 1) facilitates this bleeding by directing the bled water into the bottom tank.

BIBLIOGRAPHY

(1) Daily, J. W., "The Water Tunnel as a Tool in Hydraulic Research", Proceedings, Third Hydraulic Conference, Bulletin No. 31, State University of Iowa, 1946.

(2) Daily, J. W., Deemer, K. C., and Keller, A. L., "The Unsteady Flow Water Tunnel at the Massachusetts Institute of Technology", M.I.T. Hydrodynamics Laboratory Technical Report No. 2, 1951 (Prepared under contract with Office of Naval Research)

(3) von Karman, Th., "Turbulence and Skin Friction", Jr. Aero. Sci., Vol. 1, No. 1, January 1934.

(4) Boussinesq, J., Hydrodynamique Comptes Rendus, t. 110, 1890, pp. 1160, 1238; t. 113, 1891, pp. 9, 49.

(5) Schiller, L., "Die Entwicklung der Laminaren Geschwindigkeitsverteilung und ihre Bedeutung für Zähigkeitsmessungen. Zs. f. angew. Math. u. Mech., Bd. 2, Heft 2, pp. 96-106.

(6) Langhaar, H. L., "Steady Flow in the Transition Length of a Straight Tube", Jour. Ap. Mech., Vol. 9, No. 2, 1942.

(7) Tetervin, N., "A Review of Boundary Layer Literature", N.A.C.E. Technical Note No. 1384, July 1947.

(8) Grace, S. F., "Oscillatory Motion of a Viscous Liquid in a Long Straight Tube", Philosophical Magazine 5, 1928, p. 933.

(9) Valensi, J., "Oscillations d'un liquide pesant et visqueux dans un tube en U de faible diameter", Comptes Rendus de l'Academie des Sciences, 224, 1947, pp. 446, 532, 893, 1695.

(10) Schönfeld, J. C., "Resistance and Inertia of the Flow of Liquids in a Tube or Open Canal", Applied Science Research (Netherlands), Section A-Mechanics and Heat., Vol. 1, No. 13, 1948.

(11) Tulin, M. P., "A Study of Laminar Incompressible Viscous Flows Including Unsteady Effects", S. M. Thesis, M. I. T. , 1949

(12) Prandtl, L., "The Mechanics of Viscous Fluids", Vol. III of Aerodynamic Theory, Division G, W. F. Durand, ed. Julius Springer (Berlin) 1935.

(13) Deemer, K. C., "Fluid Friction Due to Unsteady Flow in Conduits", Sc.D. Thesis, M. I. T., 1952.

(14) Nikuradse, J., "Uber turbulente Wasserstromungen in geraden Rohren bie sehr grossen Reynoldsschen Zahlen," Vortrage aus dem Bebiete der Aerodynamik und Verwaddter Gebiete, Aachen, 1929.

(15) Nikurandse, J., "Gesetzmässigkeiten der Turbulenten Strömung in Glatten Rohren", Forschungsarbeiten des Verein Deutscher Ingenieure, H. 356, 1932.